

Visualizing the Seasonality of the Younger Dryas in Eastern North America

Ashley Cofrin
Senior Thesis
The Williams Lab
Geography Department
University of Wisconsin – Madison
May 23, 2020

Abstract

The Younger Dryas was a brief and abrupt climate event associated with a sudden cooling and drying in regions throughout the Northern Hemisphere; likely initiated by a weakening of the Atlantic meridional overturning circulation (AMOC). I analyze the effects of AMOC weakening and insolation seasonality on climate patterns in eastern North America using simulations of an Earth System Model. In addition to a forced weakening of the AMOC through a freshwater forcing in the North Atlantic, these simulations also include three experiments with obliquity and precession orbital parameters varied to minimize and maximize Northern Hemispheric insolation seasonality. While most of the hemisphere underwent cooling, eastern North America shows some signs of warming and increased precipitation following hosing. As Northern Hemisphere insolation seasonality is forced to increase temperature and precipitation seasonality decrease following hosing. Reduced temperature seasonality in eastern North America is a result of positive temperature anomalies in winter and a common cooling in summer across all orbital configuration experiments. Precipitation seasonality is reduced in all experiments from a common year-round wetting after hosing. These climate responses suggest that a weakening of the AMOC can ameliorate climate seasonality in some regions.

Introduction and Background

The Younger Dryas (YD) was a brief and abrupt climate event spanning from 12.9 ka to 11.7 ka (Rasmussen et al., 2006), during the transition from the most recent glacial period to the Holocene. The YD is characterized by a sudden cooling in regions throughout the Northern Hemisphere, and a similarly abrupt termination. Cooling in much of the Northern Hemisphere is contrasted by warming in the Southern Hemisphere, and is often attributed to a rearrangement of

heat energy transport by the Atlantic ocean, termed the “bipolar seesaw” (Stocker, 1998). The onset of the YD is hypothesized to be caused by a weakening or cessation of the Atlantic meridional overturning circulation (AMOC) (Boyle and Keigwin, 1987), a key mechanism in the northward transport of heat from the tropics. The AMOC is driven by the downwelling of surface ocean waters in the North Atlantic densified by buoyancy loss through evaporation and brine rejection. Geologic evidence of freshwater input into the Arctic ocean (Keigwin et al., 2018) and (Carlson, 2009) indicates that meltwater from the Laurentide Ice Sheet created a freshwater cap on the North Atlantic, leading to lower salinity of surface waters, a stable stratification of the water column, preventing the formation of North Atlantic Deep Water (NADW). The stratification of the North Atlantic weakened the AMOC, and cooled adjacent regions, such as Greenland. This initial cooling was then transported by changes in ocean and atmospheric circulation, leading to a change in global climate (Cheng et al., 2020).

Earth system model (ESM) simulations highlight a more spatially heterogeneous climate response to the YD than suggested by the bipolar seesaw hypothesis. Several regions demonstrate variable responses to an AMOC weakening (Kageyama, et al., 2013) and are particularly important in understanding YD climate evolution, as differing climate mechanisms are attributed to climate model disagreement. Recent temperature reconstructions from eastern North America demonstrate a dipole in temperatures during the YD (Fastovich, et al., 2020). Sites more adjacent to the North Atlantic record a cooling with the onset of the YD while sites south of Virginia demonstrate a no YD cooling (Fastovich, et al., 2020). Within eastern North America, simulated precipitation changes are strikingly consistent in comparison to simulated temperatures and suggest a wetter climate (Kageyama, et al., 2013). While the fossil-pollen record shows the increase of *Pinus*, suggesting a drier climate in parts of the eastern US, they

also expose regional differences in vegetation from different combinations of seasonal temperature and moisture-balance change (Shuman, et al., 2002). Despite some agreement among models and proxies, these simulated increases in annual precipitation overlook the importance of seasonality in storm track routing by the Laurentide Ice Sheet (Bromwich, et al., 2004). The impact of the storm track routing includes heat transport and importation into the region of study.

Seasonality of the YD has been in question due to mismatches between ice core and moraine records in comparison with snowline changes in East Greenland, northern Europe, and North America (Denton, et al., 2005). Multi-proxy temperature reconstructions and simulations from Earth system models (ESM) demonstrate that the YD likely had considerably colder winters but warmer summers in Europe than prior to AMOC weakening (Schenk, et al., 2018). In addition, winter cooling is argued to affect precipitation in Europe due to the reduced moisture uptake from the sea surface (Baldini, et al., 2019). This transition to a more continental climate is attributed to atmospheric blocking preventing the advection of colder conditions from the midlatitudinal Atlantic. Enhanced seasonality is likely not unique to Europe as mesoscale weather models under Last Glacial Maximum boundary conditions simulate a strong seasonality to mean storm track positions in eastern North America, yet, the relative importance of seasonal cycle and AMOC-induced temperature change remain unexamined.

I use several ESM simulations under various orbital configurations to disentangle the relative importance of seasonality in temperature and precipitation changes following a weakening of the AMOC and place emphasis on changes in eastern North America. Each of these simulations were performed using the Geophysical Fluid Dynamics Laboratory (GFDL) Climate Model v2 at coarse resolution ESM with constant boundary conditions and freshwater

input, but with variable obliquity and precession parameters (Delworth et al. 2006). Varying obliquity and precession produced experiments where seasonality was at a minimum and maximum in the Northern Hemisphere. These simulations demonstrate that the AMOC induces a strong climatic response in eastern North America with broad warming in the winter season and wetting throughout the year. Changing orbital configurations enhances some patterns of temperature and precipitation change, while tempering others.

Methods

Earth System Model and Experiment Description

Climate simulations were performed by Galbraith, et al. (2011) using the Geophysical Fluid Dynamics Climate Model v2 at coarse resolution. The atmospheric model has a horizontal resolution of 2.5 degrees longitude by 2.0 degrees latitude with 24 vertical levels, and an oceanic resolution of 1° in the east–west direction and varying in the north-south direction from 1 degree in the polar regions to 1/3 of a degree along the equator (Anderson, et al., 2004). Hosed conditions in the model represent a freshwater perturbation of 1.0 Sv that is input uniformly into 50°–70°N of the North Atlantic for 100 years (Galbraith, et al. 2011). Accuracy with investigating the ENA near the coast is enhanced, due to land grid cells being reduced in areas of overlapping ocean cells, so that the land and ocean perfectly tile the coast (Delworth et al., 2006). This simulation uses the Palaeoclimate Modelling Intercomparison Project (PMIP2) ice sheet boundary conditions, which places the ice sheets farther north than what is accurate for the time that the YD occurred (Braconnot, et al., 2001). CM2Mc uses Sea Ice Simulator (SIS), a dynamical model with three vertical layers, one snow and two ice, and five ice thickness categories (Delworth, et al., 2006).

Three experiments are simulated with orbital configurations (Table 1) that alter the strength of Northern Hemisphere insolation seasonality (Figure 2). A higher obliquity means the earth is at a stronger tilt and therefore intensifying the seasonality of insolation. Precession describes the movement of solstices and equinoxes relative to aphelion and perihelion. The higher degree of precession will lead to more extreme seasons as well. Hereafter, these experiments will be referred to as *high*, *medium*, and *low* corresponding to the forced Northern Hemispheric insolation seasonality.

Results And Discussion

Effect of orbital configuration on seasonal temperature and precipitation

The change in precipitation across orbital configurations simulates year round wetting in ENA (Figure 1); the pattern of drying and wetting is specific to each season, while orbital configurations modify the magnitude of the patterns. In the ENA, orbitally induced variation is greatest in winter with a 2.5 mm/day increase in the low configuration; the *high* and *low* orbital configuration experiments are similar, while *medium* shows a smallest wetting. A common, isolated, but large wetting is present in the NEUS across all orbital configurations, especially in the *low* and *high* experiments. Spring also has consistent wetting but the magnitude is lower while the spatial extends as far west as Michigan and as far south as the east coast. All orbital configurations simulate a common lack of change in precipitation during the summer, perhaps a result of common atmospheric mechanisms.

The coherent change in precipitation across orbital configurations contrasts temperature changes, where winter and spring simulate variable positive temperature anomalies in response to varied orbital configuration, while summer and fall exhibit little to no change (Figure 3). Orbitally induced variation is greatest in winter with a 5 K difference among the experiments in

the northeastern United States (NEUS), but little variability elsewhere in Eastern North America. The *high* configuration simulates the greatest positive temperature anomaly in the NEUS, while *medium* the least. Simulated spring temperature exhibits the greatest spatial variation, with positive temperature anomalies in most of ENA in the *high* and *medium* configurations. These positive temperature anomalies are greatly reduced under the *low* configuration; instead negative temperature anomalies are simulated in Florida and regions adjacent to the Gulf of Mexico. Across all orbital configurations and seasons, the greatest positive temperature anomalies are consistently in the NEUS, and likely attributed to anomalous heat transport from lower latitudes as demonstrated by anomalous transport by surface winds, along with direct radiative forcing from insolation (Figure 4). Notably, simulated summer temperatures demonstrate a common negative temperature anomaly across ENA of similar magnitude in each orbital configuration. The modern midlatitudinal and subtropical jets are strongest in the winter season, owing to a large temperature gradient across the Northern Hemisphere. Using these same simulations as I do here, McGee et al., (2018) demonstrated that simulated wetting in the western U.S. is caused by a strengthening of the subtropical jet, but limited their analysis to mean annual conditions. Surface wind anomalies suggest that the subtropical jet may also be responsible for drawing heat into ENA, particularly in spring and winter when the modern jets are the strongest (Bjerknes, 1964) and anomalous southerly transport is the greatest in the simulations (Figure 4; McGee et al., 2018). The modern climatology of ENA identifies midlatitude jet stream strength, configuration, and position as a mechanism for controlling southerly transport into ENA and supports this analysis (Deser, et al., 1993). A seasonal weakening of the Northern Hemispheric jets during the summer may reduce this heat transport equally across each experiment. Reduced heat transport and a common negative radiative forcing in the North Hemisphere from an AMOC

shutdown (Gailbraith et al., 2016) may then produce the consistent simulated summer cooling exhibited across all experiments.

A common Last Glacial Maximum ice sheet configuration across all experiments (Figure 5) may be responsible for some of the common variations across the experiments. In all orbital configurations, high pressure glacial anticyclones formed over the Laurentide Ice Sheet during the summer months and is associated with northerly katabatic winds flowing off of the ice sheet into ENA (Bromwich, et al., 2005). Simplified three-dimensional coupled ice sheets–stationary wave model's show that the ice sheet topography induces an anticyclonic circulation over the ice sheet, causing a slight warming over the western slopes and a stronger cooling over the remainder (Roe and Lindzen, 2001). Brownwich, et al. (2002) confirms that continental ice sheet topography exerts a primary influence on the stationary wave pattern, which in turn determines the patterns of temperature over the ice sheet with a specific focus on modeling the Laurentide Ice Sheet; due to the ice sheets proximity to eastern North America, some variation can be rooted from the ice sheet.

Seasonality amelioration facilitated by AMOC weakening

Seasonality in temperature in ENA is decreased in response to increasing insolation seasonality and is caused by anomalous warming in winter and cooling in summer. Among the three orbital configurations, insolation seasonality (i.e. difference between mean summer and mean winter insolation) varies by as much as 200 W m^{-2} in eastern North America (Figure 2). The *high* experiment forces the greatest difference in summer and winter insolation of $\sim 300 \text{ W m}^{-2}$ while the *low* experiment has a forced insolation seasonality of 100 W m^{-2} . Despite increasing insolation seasonality, positive temperature anomalies during winter and negative temperature anomalies during summer indicate that temperature seasonality is reduced in eastern

North America (Figure 6). This pattern is particularly strong in the northeastern United States where the summer-winter temperature difference decreases by as much as 4 K under the *high* configuration but only decreases by 3 K under the *low* configuration (Figure 6). Notably, this decrease in temperature seasonality in response to increased insolation seasonality does not vary linearly. The *medium* configuration includes a forced insolation seasonality of ~250 Wm-2, and regions of eastern North America such as the Great Lakes region and Florida simulate increased temperature seasonality following hosing (Figure 6). This suggests that a shutdown of the AMOC ameliorates the forced increase in insolation seasonality, likely through regional changes in atmospheric circulation. Surface wind anomalies demonstrate the strongest southerly transport in the *high* experiment and the weakest in the *medium* experiment, but all experiments demonstrated a lack of southerly transport in the summer season (Figure 4), similar to the patterns in decreased temperature seasonality. A similar regional atmospheric response is also present in proxy and ESM simulations in Europe. A weakening of the AMOC increased summer temperatures but decreased winter temperatures, increasing temperature seasonality (Schenk, 2018). This pattern was caused by an enhanced glacial anticyclone over the Fennoscandian ice sheet during the summer months, blocking cold winds off the North Atlantic from penetrating the European midcontinent.

Strength of season

Anomalies show that there is a misalignment with the orbital configurations we expected to see the highest seasonal response in, and what is shown. To determine seasonal responses, we subtracted the summer anomaly plot by the winter anomaly plot for each orbital configuration for both temperature and precipitation; these new anomalies show the differences of summer versus winter. Negative numbers are indicative of summer and winter temperatures being similar

following hosing, meaning a lower seasonal response; and positive values indicate a high seasonal response (Figure 6). Under these conditions medium orbital configuration shows the highest seasonal response for both temperature and precipitation in the ENA. The temperature in the medium experiment shows increasing differences between the changing seasons (increasing seasonality), while low and high have decreasing seasonality. These results are surprising as we expected to see an increase in seasonal responses as the orbital configuration got higher. The precipitation plots also display a high seasonal response in the medium orbital configuration, while the highest orbital configuration shows the lowest seasonal response. Specifically, In Maritime Canada, precipitation changes heavily between summer and winter after hosing. In the ENA, summer and winter are similar after hosing; meaning that the changing season is not very impactful on precipitation levels.

Conclusion

I analyse the effects of AMOC weakening during the Younger Dryas period alongside three experiments with obliquity and precession orbital parameters varied to minimize and maximize Northern Hemispheric insolation seasonality. As Northern Hemisphere insolation seasonality is forced to increase temperature and precipitation seasonality decrease following hosing. Reduced temperature seasonality in eastern North America is a result of positive temperature anomalies in winter and a common cooling in summer across all orbital configuration experiments. Precipitation seasonality is reduced in all experiments from a common year-round wetting after hosing. These climate responses suggest that a weakening of the AMOC can ameliorate climate seasonality in some regions.

Moving Forward

The ESM simulations used here provide important insight into relevant temperature and precipitation patterns in eastern North America following a weakening of the AMOC, but need independent assessment from proxy data. Eastern North America has hundreds of temperature and precipitation sensitive fossil-pollen records (Williams, et al., 2018) that can be used to assess the accuracy of these simulations. Less focus has been placed on synthesizing precipitation changes to the Younger Dryas in eastern North America which can provide insights into relevant atmospheric dynamics.

Acknowledgements

I would like to thank Professor Jack Williams and David Fastovich for their continuous support, encouragement, insights, and ideas in the development of this work. I would also like to thank the entire Williams Lab for their constant positivity and help.

Figures

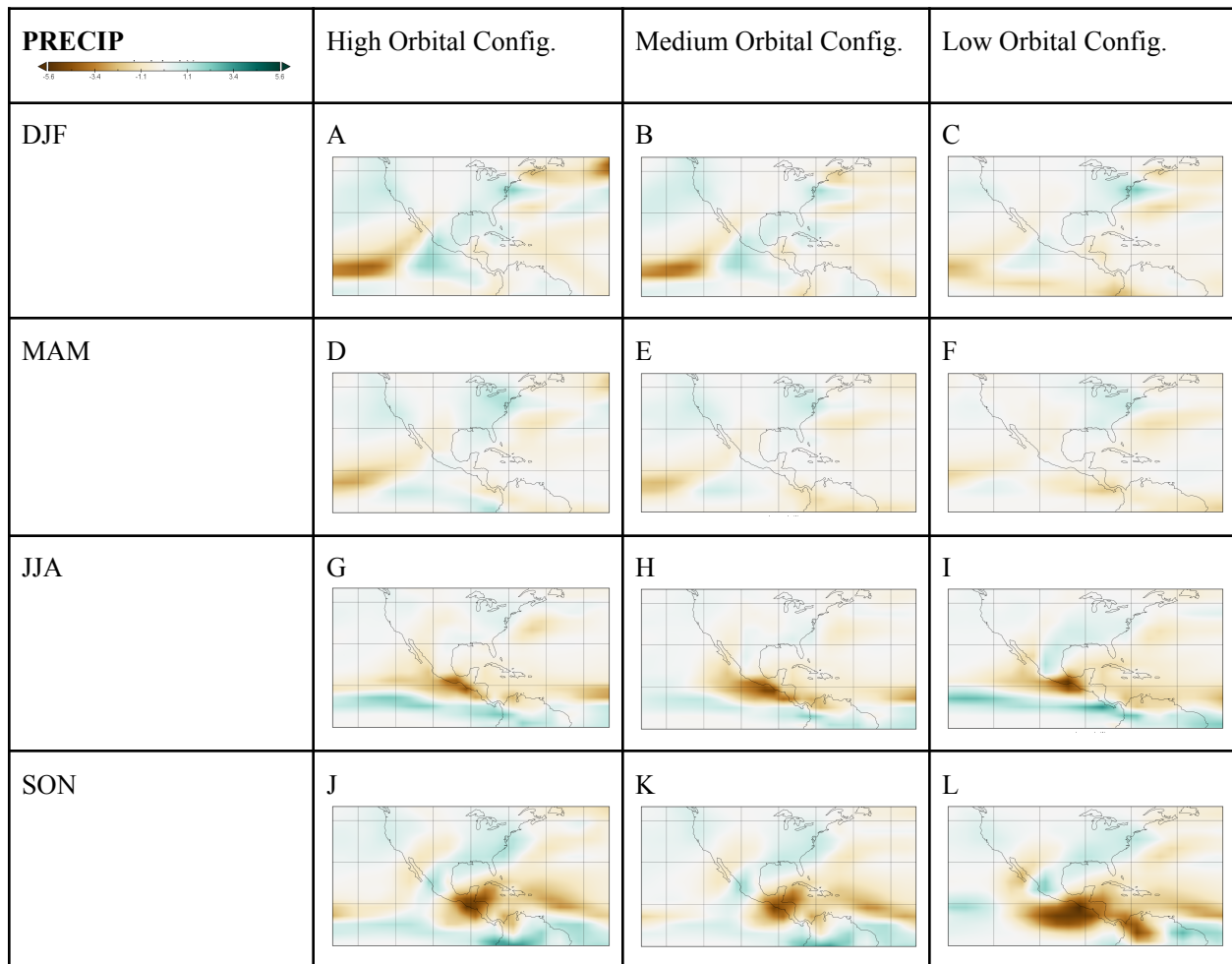


Figure 1: Precipitation anomaly plots showing ‘hosed’-‘unhosed’ conditions.

Seasonality	Earth's Obliquity and Precession.
“High”	270 precession and 24 obliquity
“Medium”	270 precession and 22.5 obliquity
“Low”	90 precession and 22.5 obliquity

Table 1: Model Configurations

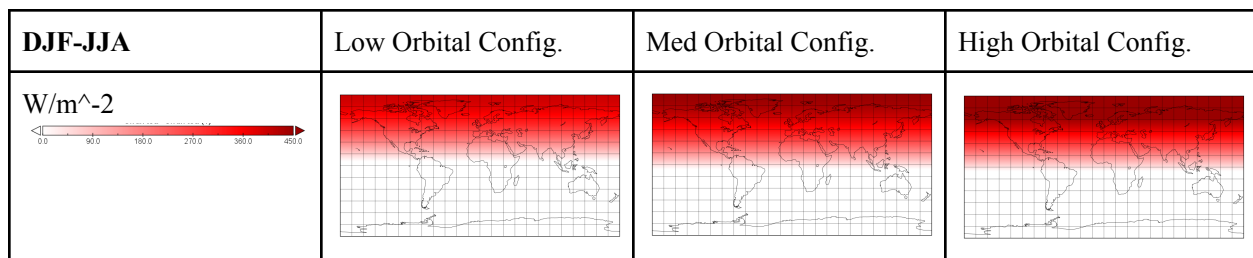


Figure 2: Shortwave flux at the top of the atmosphere. Positive numbers indicate a greater difference between summer and winter.

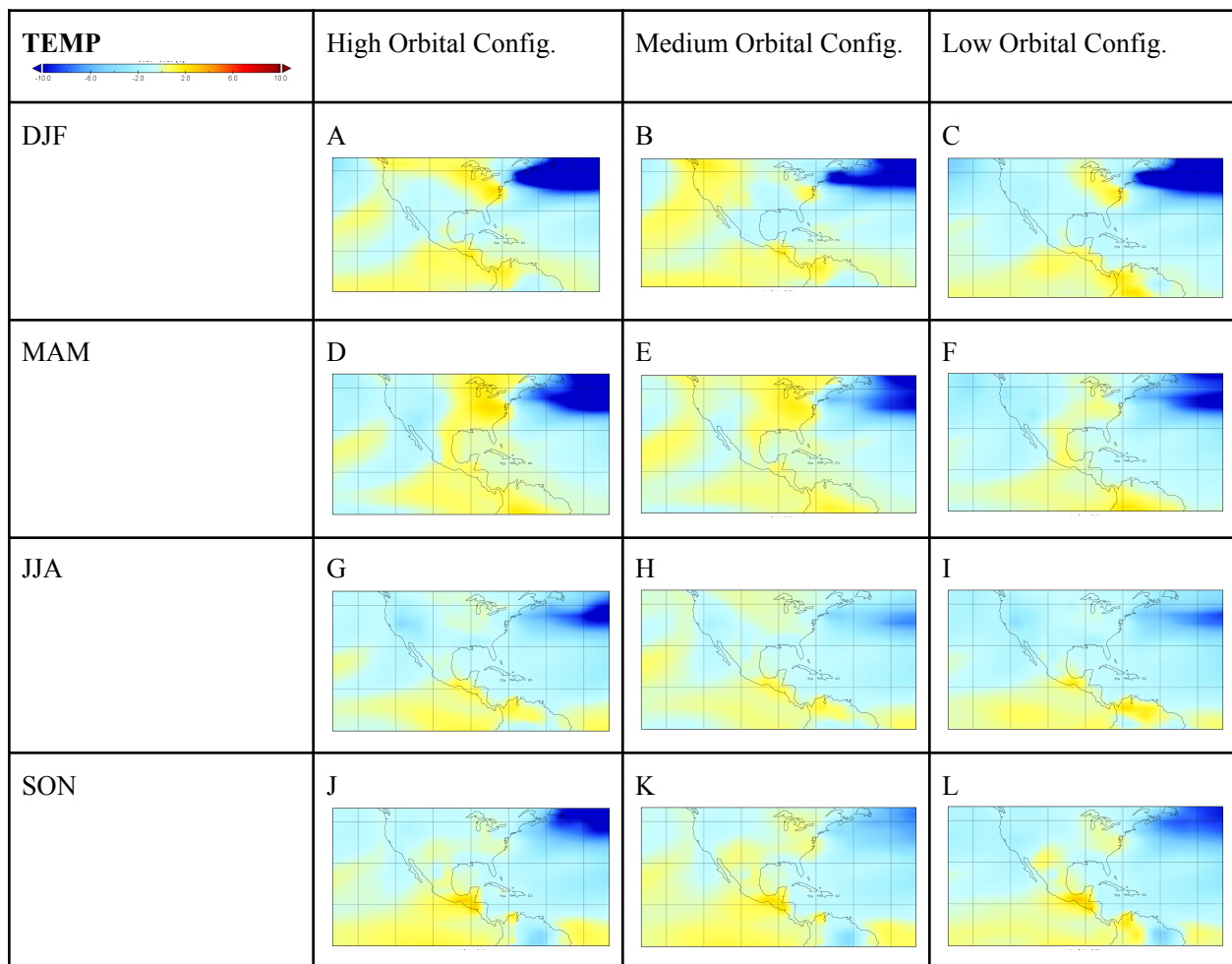


Figure 3: Temperature anomaly plots showing ‘hosed’- ‘unhosed’ conditions.

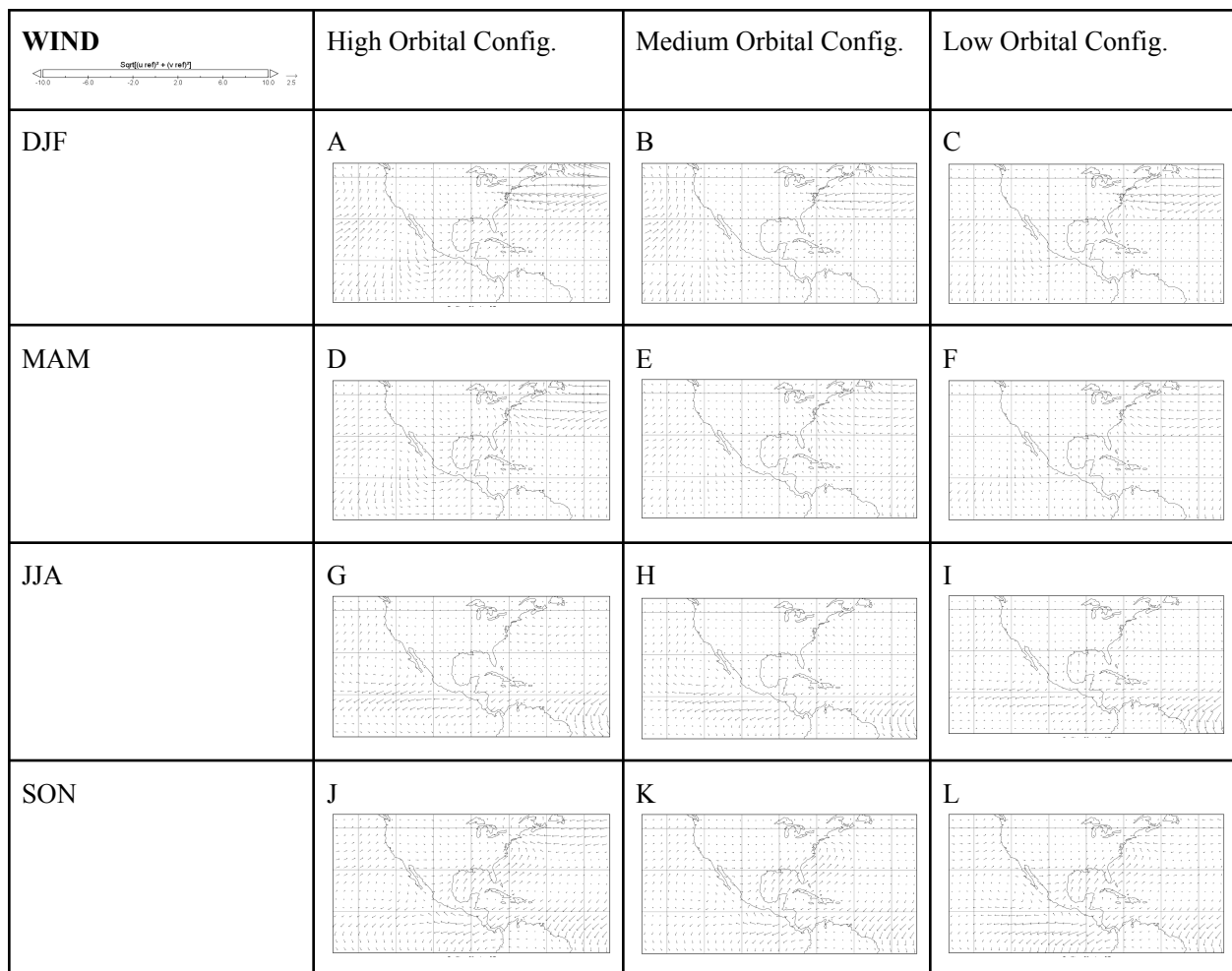


Figure 4: Surface wind anomaly plots showing ‘hosed’- ‘unhosed’ conditions.

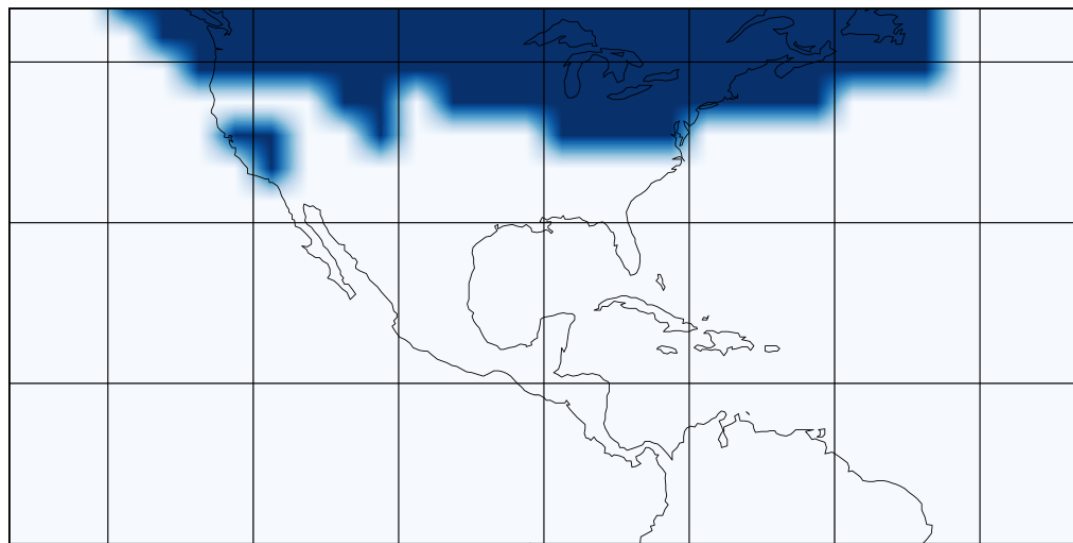


Figure 5: Ice placement.

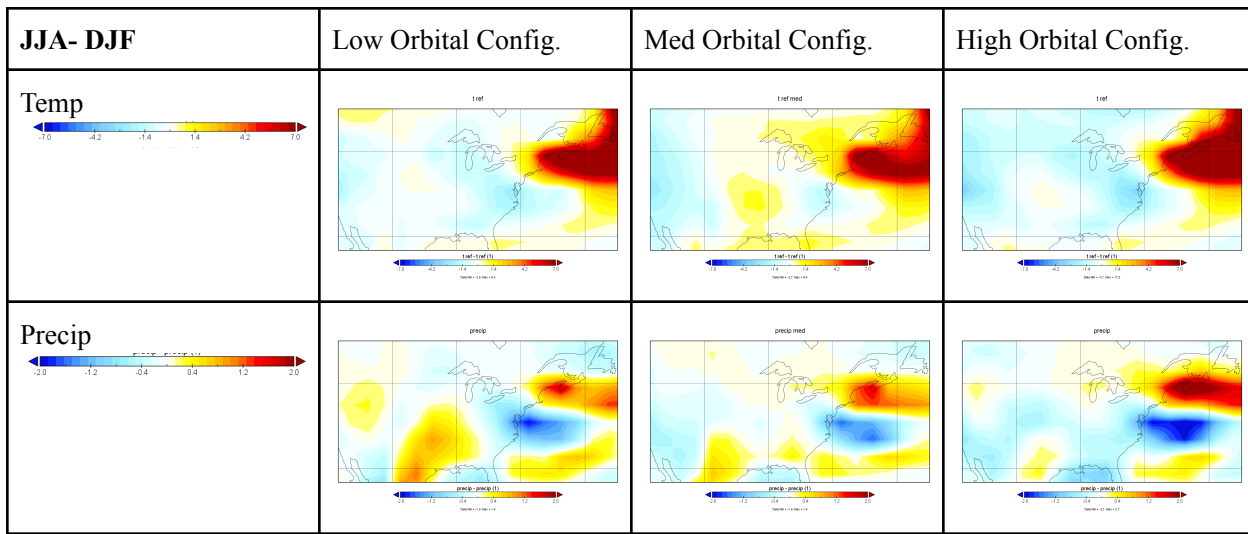


Figure 6: Difference between summer and winter temperature hosed-unhosed anomalies. Cooler colors indicate that the difference between summer and winter temperature decreases following hosing. Warmer colors indicate that the difference between summer and winter temperatures increased following hosing. .

References

- Anderson, Jeffrey L., Broccoli, Anthony J., et al. (2004). The new gfdl global atmosphere and land model am2–lm2: Evaluation with prescribed sst simulations. *Journal of Climate*, 17(24), 4641-4673. doi:10.1175/jcli-3223.1
- Bartlein, P. J., Harrison, S. P., Brewer, S., Connor, S., Davis, B. A., Gajewski, K., Wu, H. (2011). Pollen-based continental climate reconstructions at 6 and 21 KA: A Global Synthesis. *Climate Dynamics*, 37(3-4), 775-802. doi:10.1007/s00382-010-0904-1
- Baldini, L. M., Baldini, J. U., McDermott, F., Arias, P., Cueto, M., Fairchild, I. J., Richards, D. A. (2019). North Iberian temperature and rainfall Seasonality over the Younger Dryas and Holocene. *Quaternary Science Reviews*, 226, 105998. doi:10.1016/j.quascirev.2019.105998
- Bjerknes, J. (1964). Atlantic Air-Sea Interaction, in: Landsberg, H.E., Van Mieghem, J. (Eds.), Advances in Geophysics. *Academic Press*, New York, pp. 1-82.
- Boyle, E., Keigwin, L. (1987). North Atlantic thermohaline circulation during the past 20,000 years linked to high-latitude surface temperature. *Nature* 330, 35–40.
<https://doi.org/10.1038/330035a>
- Braconnot, P., Otto-Bliesner, B., Harrison, S., Joussaume, S., Peterchmitt, J., Abe-Ouchi, A., . . . Zhao, Y. (2007). Results of pmip2 coupled simulations of THE mid-holocene and last Glacial Maximum – Part 1: Experiments and large-scale features. *Climate of the Past*, 3(2), 261-277. doi:10.5194/cp-3-261-2007

Bromwich, D. H., Toracinta, E. R., Wei, H., Oglesby, R. J., Fastook, J. L., & Hughes, T. J. (2004). Polar MM5 simulations of the winter climate of the Laurentide ice sheet at the LGM*. *Journal of Climate*, 17(17), 3415-3433. doi:10.1175/1520-0442(2004)0172.0.co;2

Bromwich, D.H., Toracinta, E.R., Oglesby, R.J., Fastook, J.L., Hughes, T.J. (2005). LGM summer climate on the southern margin of the Laurentide Ice Sheet: Wet or dry? *Journal of Climate* 18, 3317-3338.

Brown, N. and Galbraith, E. D. (2016) Hosed vs. unhosed: interruptions of the Atlantic Meridional Overturning Circulation in a global coupled model, with and without freshwater forcing, *Clim. Past*, 12, 1663–1679, <https://doi.org/10.5194/cp-12-1663-2016>.

Cheng, Hai and Zhang, Haiwei, et al., (2020). Timing and structure of the Younger Dryas event and its underlying climate dynamics. *National Academy of Sciences*, 117, 38, 23408--23417, 10.1073/pnas.2007869117.

Carlson, A. E. (2009). What caused the younger dryas cold event? *Geology*, 38(4), 383-384. doi:10.1130/focus042010.1

Delworth, T. L., Broccoli, A. J., Rosati, A., Stouffer, R. J., Balaji, V., Beesley, J. A., . . . Zhang, R. (2006). GFDL's cm2 Global coupled climate Models. Part I: Formulation and SIMULATION CHARACTERISTICS. *Journal of Climate*, 19(5), 643-674. doi:10.1175/jcli3629.1

Denton, G. H., Alley, R.B., Comer, G. C.,and Broecker, W.S. (2005). The Role of Seasonality in Abrupt Climate Change *Quat. Sci. Rev.*, 24, pp. 1159-1182

Deser, C., & Blackmon, M. L. (1993). Surface climate variations over the North Atlantic Ocean during winter: 1900–1989. *Journal of Climate*, 6(9), 1743-1753. doi:10.1175/1520-0442(1993)0062.0.co;2

Easterling, D.R., K.E. Kunkel, J.R. Arnold, T. Knutson, A.N. LeGrande, L.R. Leung, R.S. Vose, D.E. Waliser, and M.F. Wehner, 2017: Precipitation change in the United States. In: Climate Science Special Report: Fourth National Climate Assessment, Volume I [Wuebbles, D.J., D.W. Fahey, K.A. Hibbard, D.J. Dokken, B.C. Stewart, and T.K. Maycock (eds.)]. U.S. Global Change Research Program, Washington, DC, USA, pp. 207-230, doi: 10.7930/J0H993CC.

Fastovich, D., Russell, J. M., Jackson, S. T., Krause, T. R., Marcott, S. A., & Williams, J. W. (2020). Spatial fingerprint of Younger Dryas cooling and warming in eastern North America. *Geophysical Research Letters*, 47, e2020GL090031. <https://doi.org/10.1029/2020GL090031>

Fastovich, D., Russell, J. M., Jackson, S. T., & Williams, J. W. (2020). Deglacial temperature controls on no-analog community establishment in the Great Lakes Region. *Quaternary Science Reviews*, 234, 106245. <https://doi.org/10.1016/j.quascirev.2020.106>

Galbraith, E. D., Kwon, E. Y., Gnanadesikan, A., Rodgers, K. B., Griffies, S. M., Bianchi, D., Sarmiento, J. L., Dunne, J. P., Simeon, J., Slater, R. D., Wittenberg, A. T., & Held, I. M. (2011).

Climate Variability and Radiocarbon in the CM2Mc Earth System Model, *Journal of Climate*, 24(16), 4230-4254. <https://journals.ametsoc.org/view/journals/clim/24/16/2011jcli3919.1.x>

Kageyama, M., Merkel, U., Otto-Bliesner, B., Prange, M., Abe-Ouchi, A., Lohmann, G., Ohgaito, R., Roche, D., Singarayer, J., & Swingedouw, D. (2013). Climatic impacts of fresh water hosing under Last Glacial Maximum conditions: A multi-model study. *Climate of the Past*, 9(2), 935– 953.

Keigwin, L. D., Jones, G. A., and Lehman, J. (1991). Deglacial Meltwater Discharge, North Atlantic Deep Circulation, and Abrupt Climate Change, *Journal of Geophysical Research*, 96.

Keigwin, L. D., Klotsko, S., Zhao, N., Reilly, B., Giosan, L., & Driscoll, N. W. (2018). Deglacial floods in the Beaufort SEA Preceded Younger DRYAS cooling. *Nature Geoscience*, 11(8), 599-604. doi:10.1038/s41561-018-0169-6

Lamy, F., Kaiser, J., Helge, W. Arz, Hebbeln, D., Ninnemann, U., Timm, O., Timmermann, A., Toggweiler J.R. (2007). Modulation of the bipolar seesaw in the Southeast Pacific during Termination 1, *Earth and Planetary Science Letters*, Volume 259, Issues 3–4, Pages 400-413, ISSN 0012-821X, <https://doi.org/10.1016/j.epsl.2007.04.040>.

McGee, D., Moreno-Chamarro, E., Green, B., Marshall, J., Galbraith, E., and Bradtmiller, L. (2018). Hemispherically asymmetric trade wind changes as signatures of past ITCZ shifts, *Quaternary Science Reviews* 180 (2018) 214e228.

Øyvind Lie, Øyvind Paasche. (2006). How extreme was northern hemisphere seasonality during the Younger Dryas?, *Quaternary Science Reviews*, Volume 25, Issues 5–6, Pages 404-407, ISSN 0277-3791, <https://doi.org/10.1016/j.quascirev.2005.11.003>.

Randall, D.A., R.A. Wood, S. Bony, R. Colman, T. Fichefet, J. Fyfe, V. Kattsov, A. Pitman, J. Shukla, J. Srinivasan, R.J. Stouffer, A. Sumi and K.E. Taylor (2007) Climate Models and Their Evaluation. In: Climate Change 2007: The Physical Science Basis. Contribution of Working Group I to the Fourth Assessment Report of the Intergovernmental Panel on Climate Change [Solomon, S., D. Qin, M. Manning, Z. Chen, M. Marquis, K.B. Averyt, M.Tignor and H.L. Miller (eds.)]. Cambridge University Press, Cambridge, United Kingdom and New York, NY, USA.

Rasmussen, S.O., Andersen, K.K., Svensson, A.M., Steffensen, J.P., Vinther, B.M., Clausen, H.B., Siggaard-Andersen, M.L., Johnsen, S.J., Larsen, L.B., Dahl-Jensen, D., Bigler, M., Rothlisberger, R., Fischer, H., Goto-Azuma, K., Hansson, M.E., Ruth, U. (2006). A new Greenland ice core chronology for the last glacial termination. *Journal of Geophysical Research-Atmospheres* 111, 16.

Roe, G. H., & Lindzen, R. S. (2001). The mutual interaction between continental-scale ice sheets and atmospheric stationary waves. *Journal of Climate*, 14(7), 1450-1465.
doi:10.1175/1520-0442(2001)0142.0.co;2

Schenk, F., Valiranta, M., Muschitiello, F., Tarasov, L., Heikkila, M., Bjorck, S., Brandefelt, J., Johansson, A.V., Naslund, J.O., Wohlfarth, B. (2018). Warm summers during the Younger Dryas cold reversal. *Nature Communications* 9, 13.

Shuman, B., Webb, T. III, Bartlein, P., & Williams, J. W. (2002). The anatomy of a climatic oscillation: Vegetation change in eastern North America during the Younger Dryas chronozone. *Quaternary Science Reviews*, 21(16–17), 1777–1791.
[https://doi.org/10.1016/S0277-3791\(02\)00030-6](https://doi.org/10.1016/S0277-3791(02)00030-6)

Shuman, B. (2003). Controls on loss-on-ignition variation in cores from two shallow lakes in the northeastern United States. *Journal of Paleolimnology* 30, in press.

Shuman, B., J. Bravo, J. Kaye, J. A. Lynch, P. Newby, and T. Webb, III. (2001). Late-Quaternary water-level variations and vegetation history at Crooked Pond, Southeastern Massachusetts. *Quaternary Research* 56:401-410.

Stocker, T. F. (1998). Climate change—The seesaw effect. *Science*, 282(5386), 61–62.
<https://doi.org/10.1126/science.282.5386.61>

Williams, J.W., Grimm, E.C., Blois, J.L., Charles, D.F., Davis, E.B., Goring, S.J., Graham, R.W., Smith, A.J., Anderson, M., Arroyo-Cabralles, J., Ashworth, A.C., Betancourt, J.L., Bills, B.W., Booth, R.K., Buckland, P.I., Curry, B.B., Giesecke, T., Jackson, S.T., Latorre, C., Nichols, J., Purdum, T., Roth, R.E., Stryker, M., Takahara, H. (2018). The Neotoma Paleoecology Database, a multiproxy, international, community-curated data resource. *Quaternary Research* 89, 156-177.

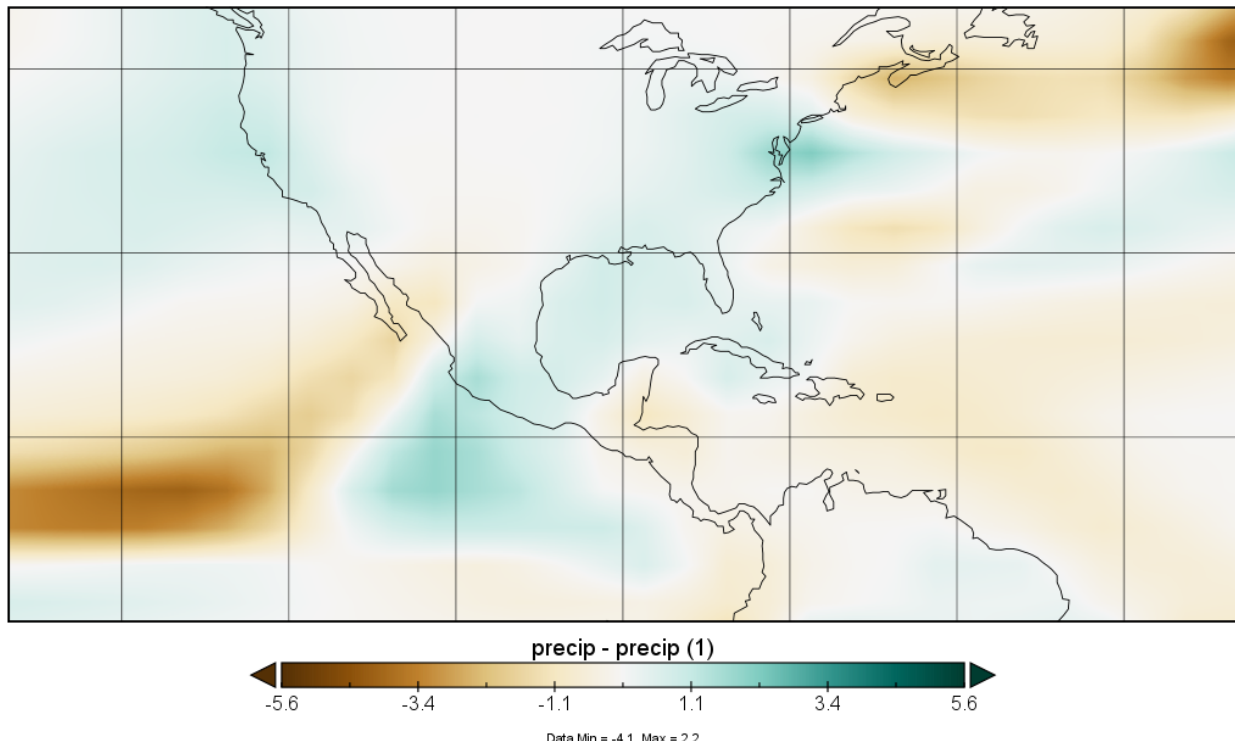
Yin, J., & Stouffer, R. J. (2007). Comparison of the Stability of the Atlantic Thermohaline Circulation in Two Coupled Atmosphere–Ocean General Circulation Models, *Journal of Climate*, 20(17), 4293–4315. Retrieved Jan 24, 2021, from
<https://journals.ametsoc.org/view/journals/clim/20/17/jcli4256.1.xml>

Zarriess, M., Johnstone, H., Prange, M., Steph, S., Groeneveld, J., Mulitza, S., and Mackensen, A. (2011). Bipolar seesaw in the northeastern tropical Atlantic during Heinrich stadials, *Geophys. Res. Lett.*, 38, L04706, doi:10.1029/2010GL046070.

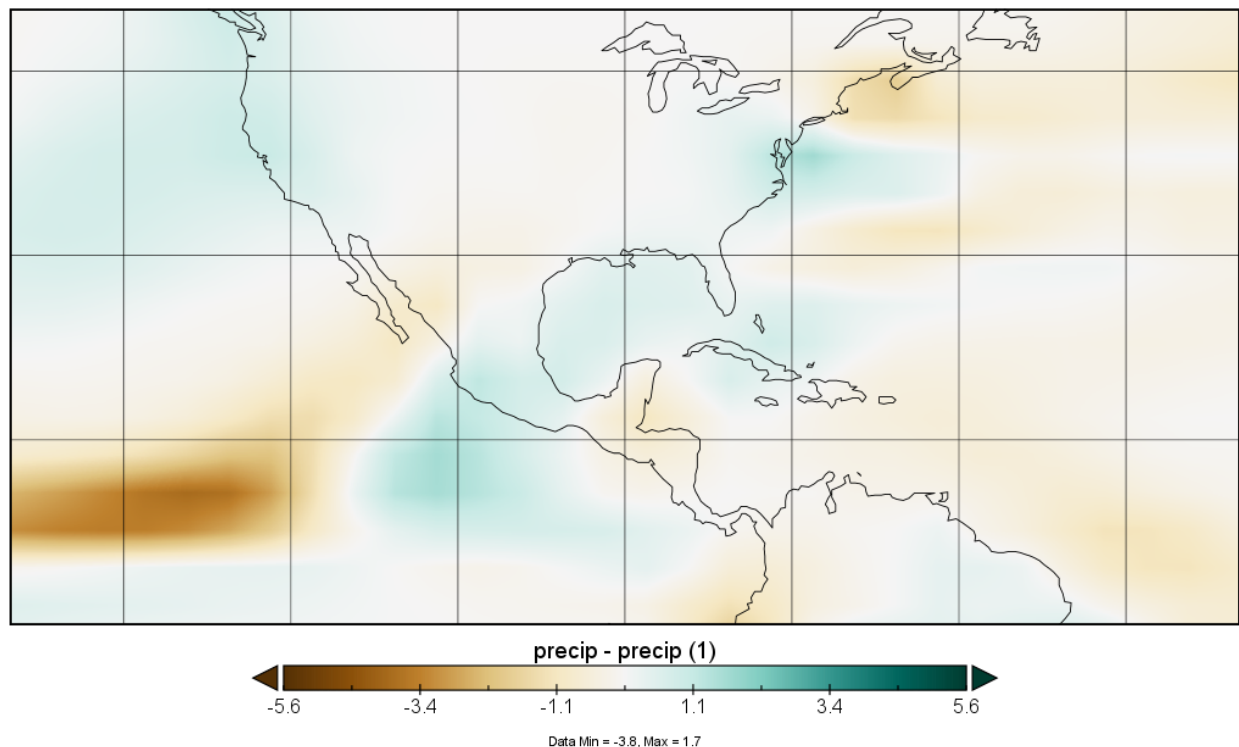
Appendix

Precipitation

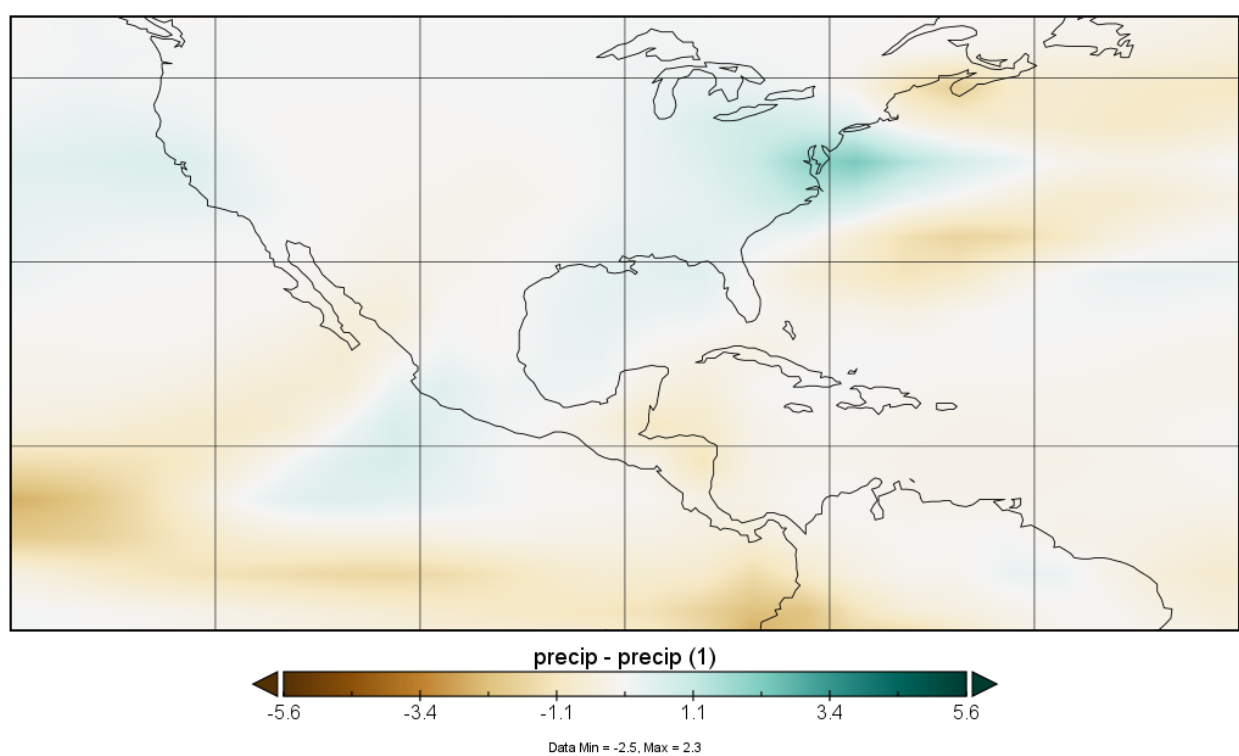
Hosed-unhosed in DJF, high orbital configuration, precipitation anomaly



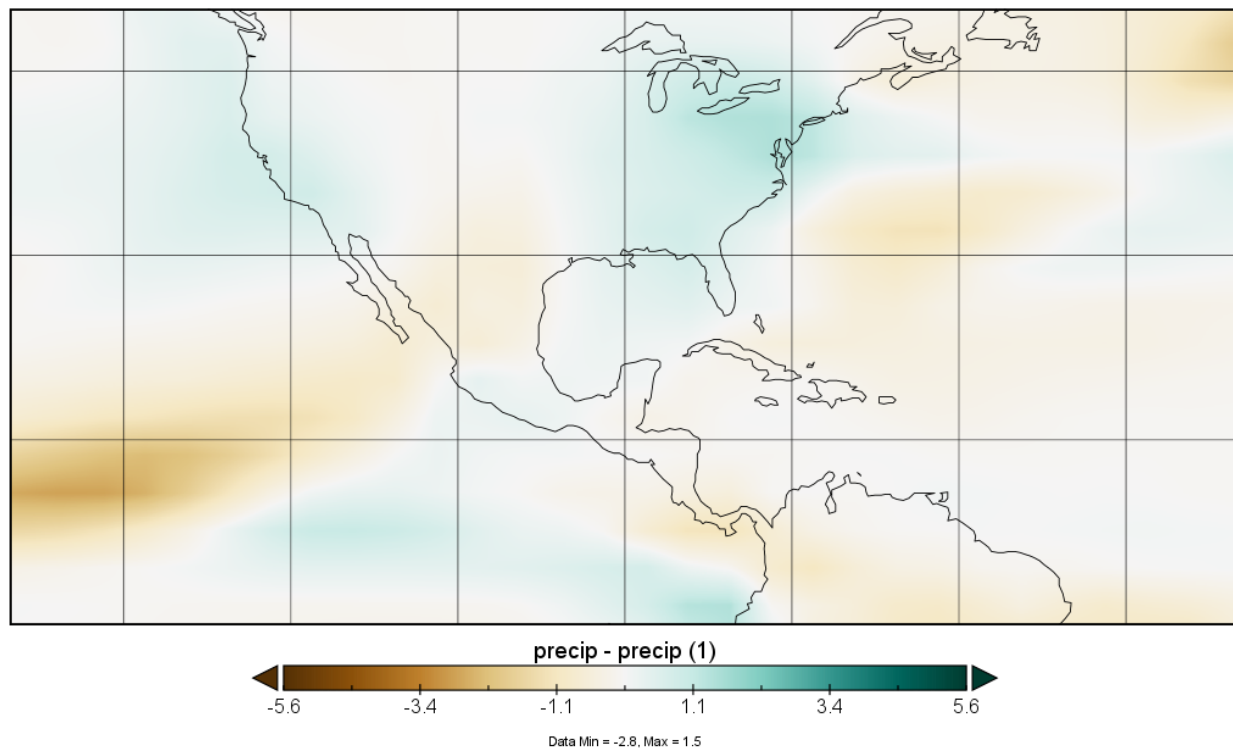
Hosed-unhosed in DJF, medium orbital configuration, precipitation anomaly



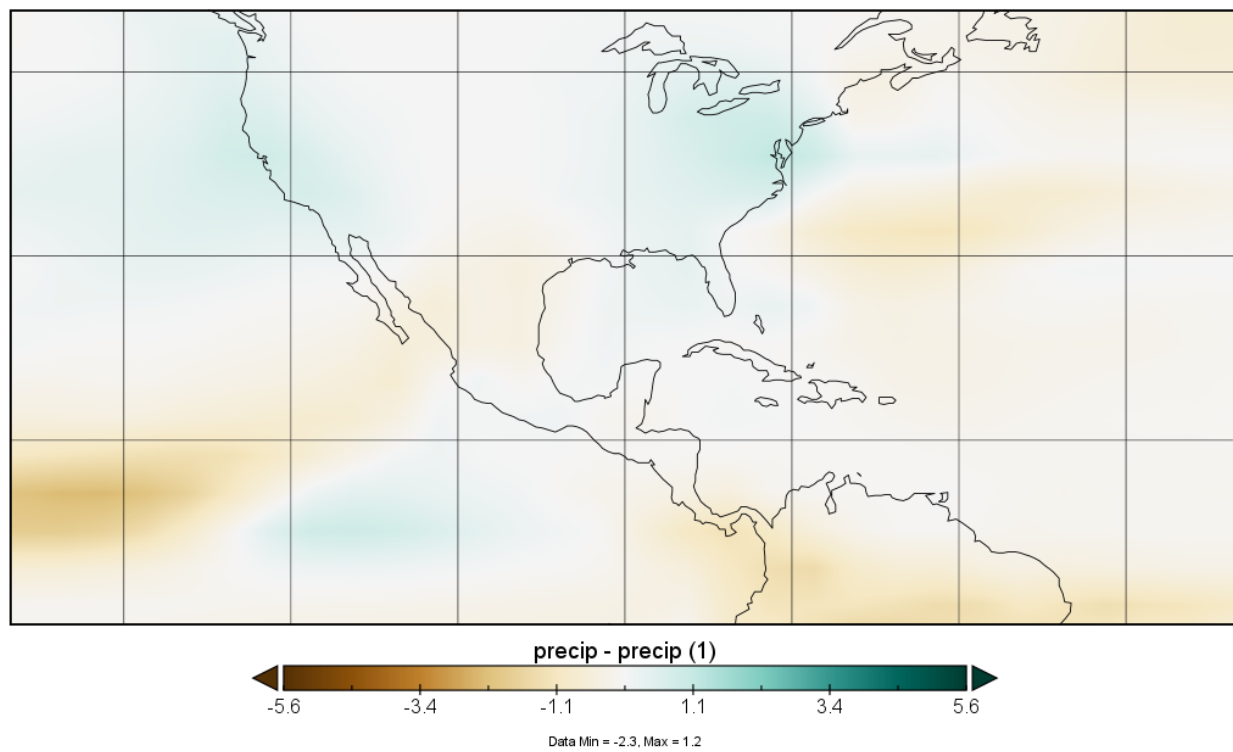
Hosed-unhosed in DJF, low orbital configuration, precipitation anomaly



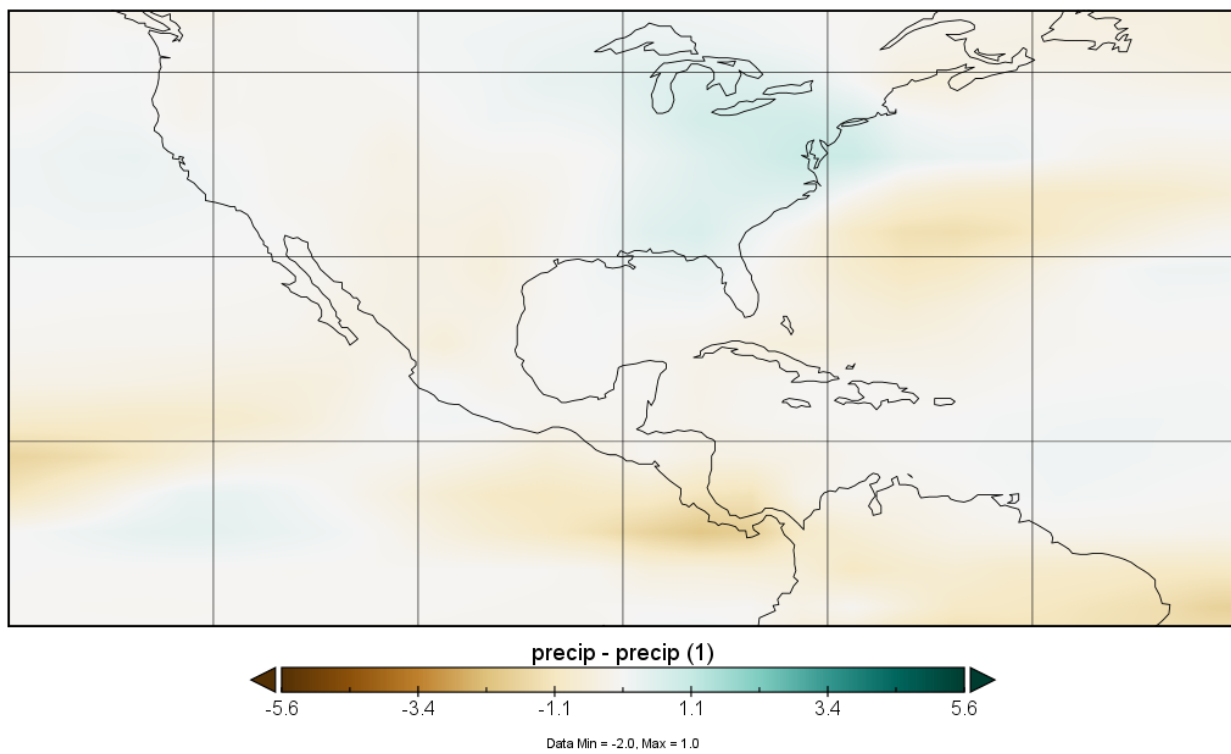
Hosed-unhosed in MAM, high orbital configuration, precipitation anomaly



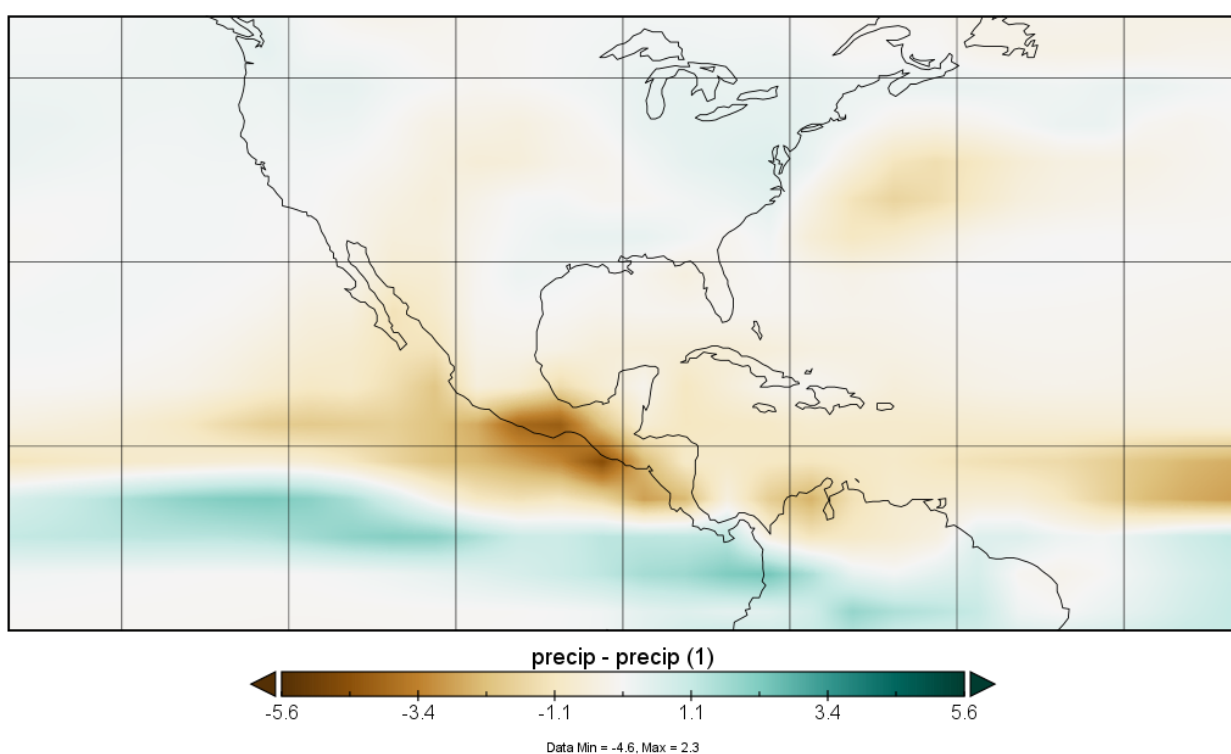
Hosed-unhosed in MAM, medium orbital configuration, precipitation anomaly



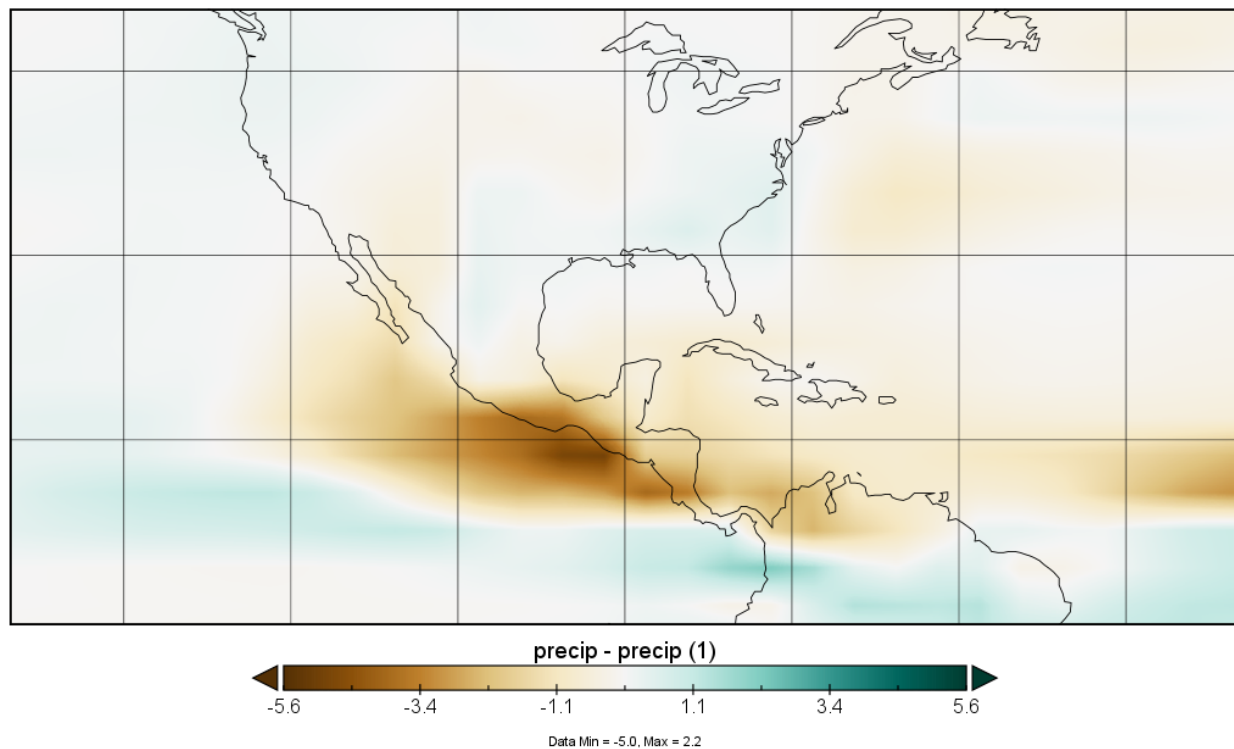
Hosed-unhosed in MAM, low orbital configuration, precipitation anomaly



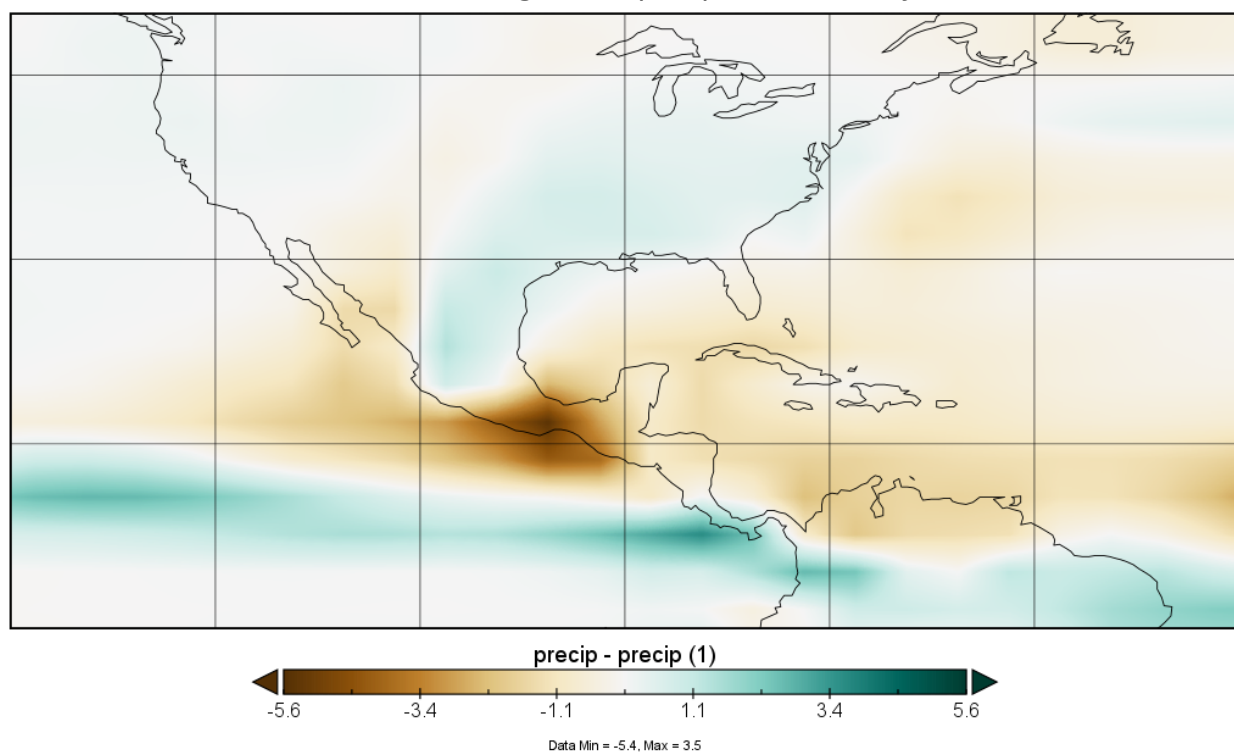
Hosed-unhosed in JJA, high orbital configuration, precipitation anomaly



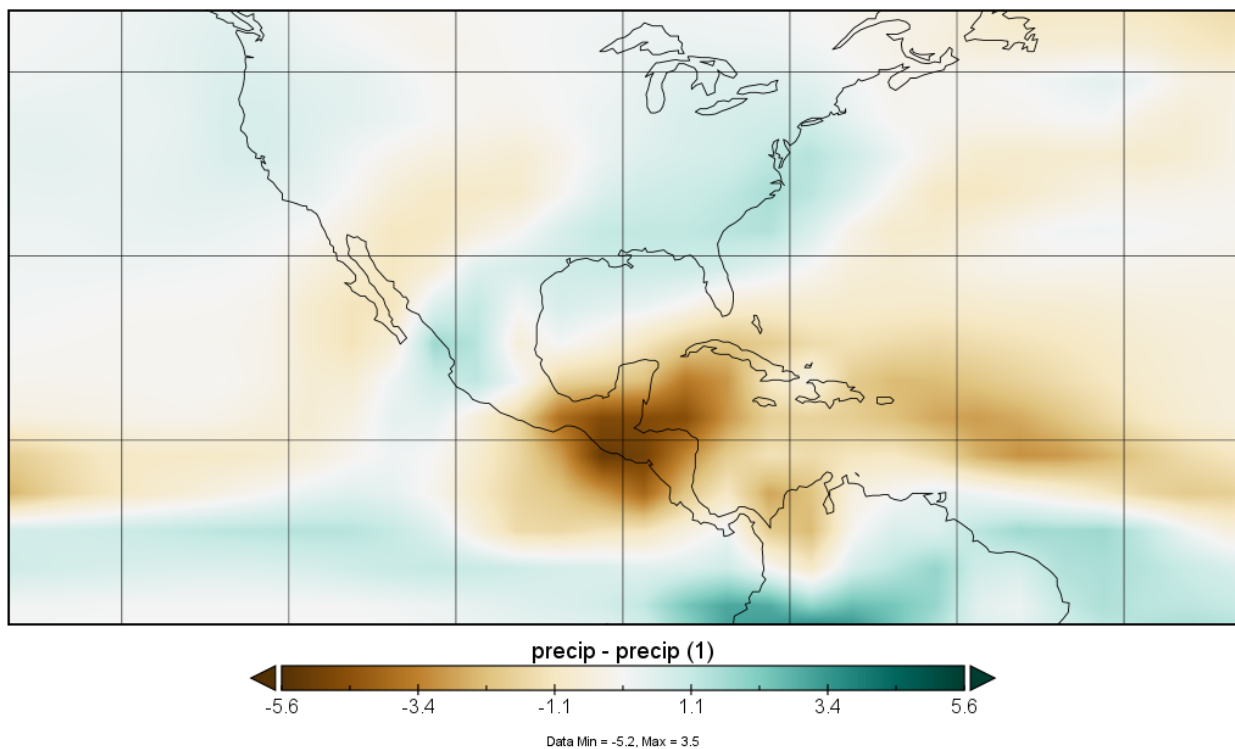
Hosed-unhosed in JJA, medium orbital configuration, precipitation anomaly



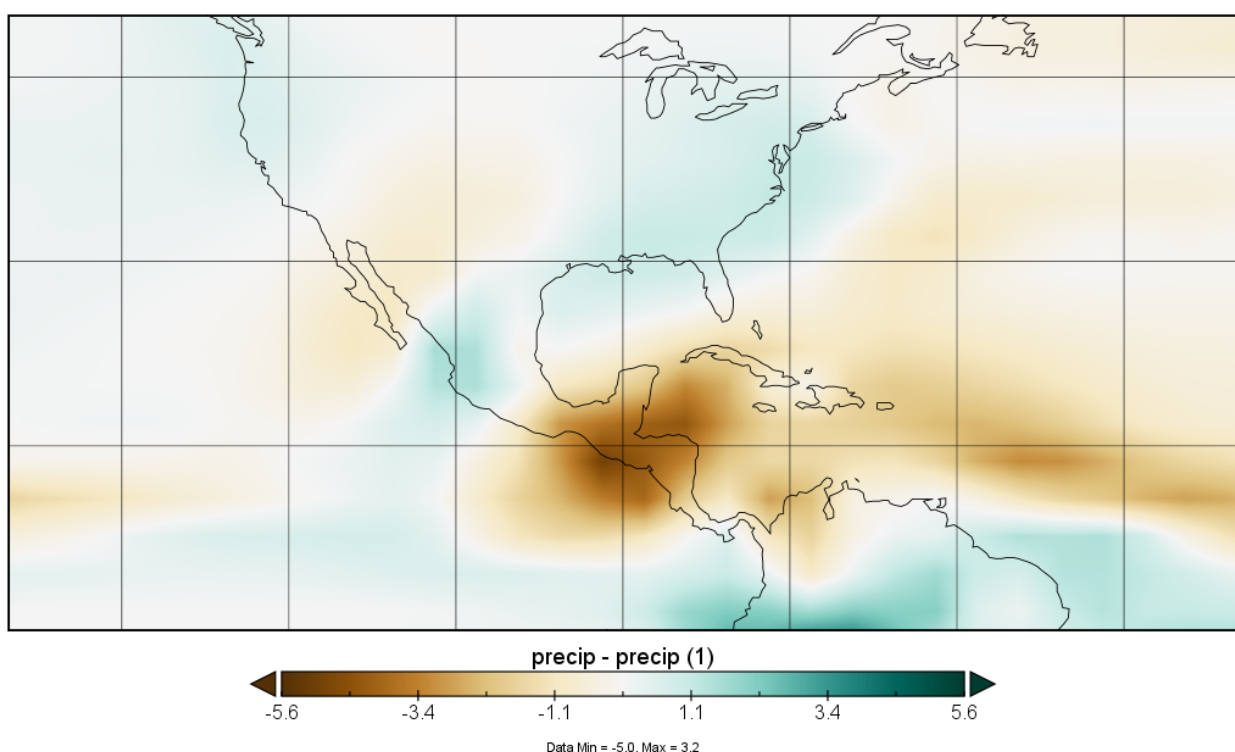
Hosed-unhosed in JJA, low orbital configuration, precipitation anomaly



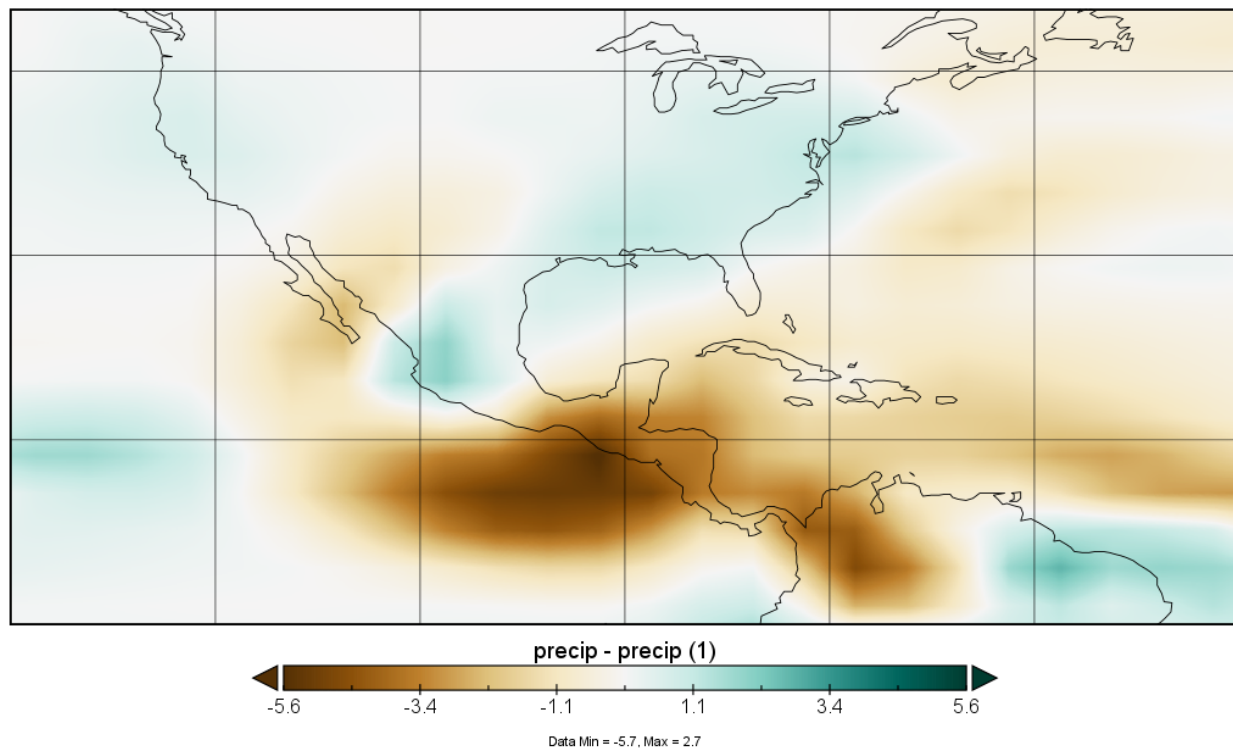
Hosed-unhosed in SON, high orbital configuration, precipitation anomaly



Hosed-unhosed in SON, medium orbital configuration, precipitation anomaly

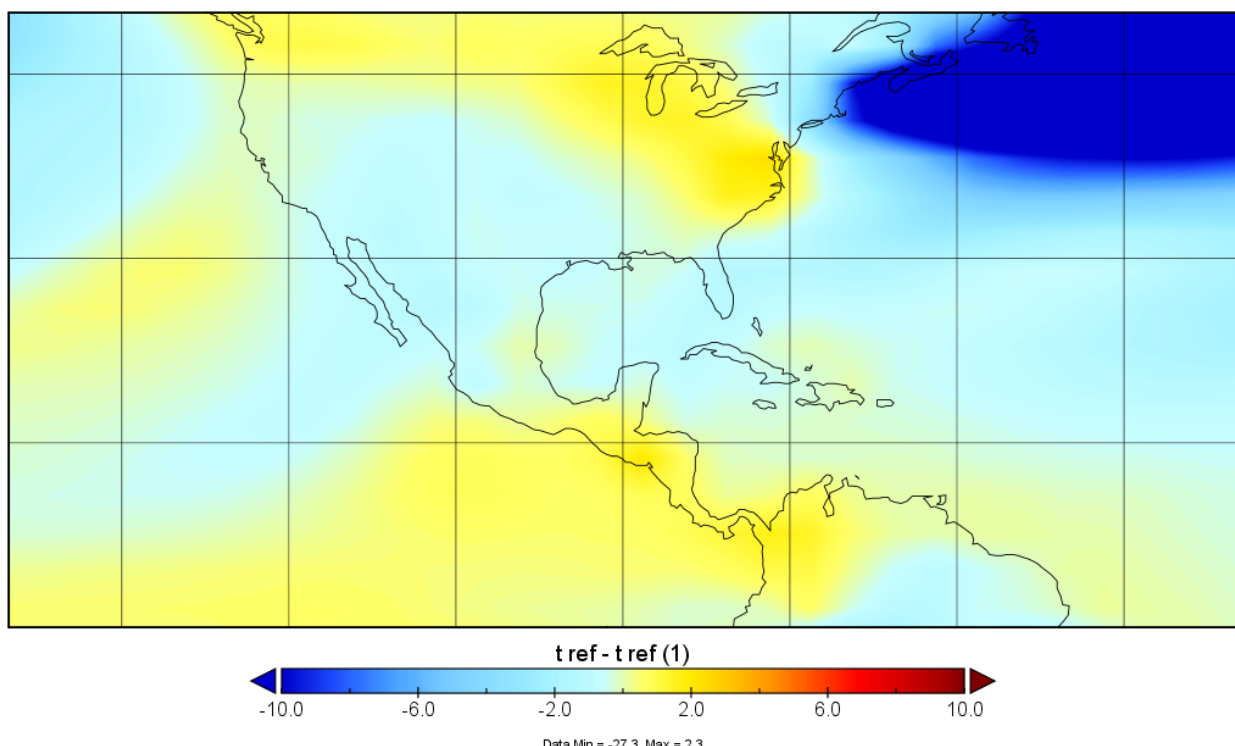


Hosed-unhosed in SON, low orbital configuration, precipitation anomaly

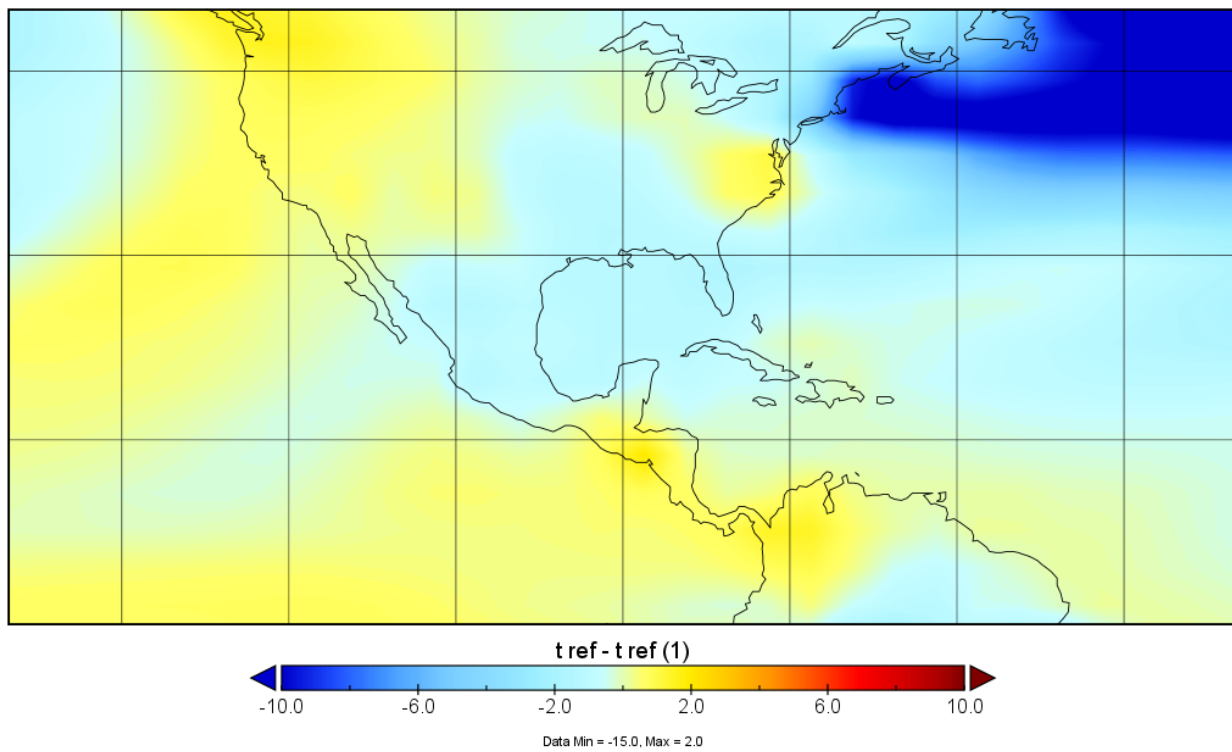


Temperature

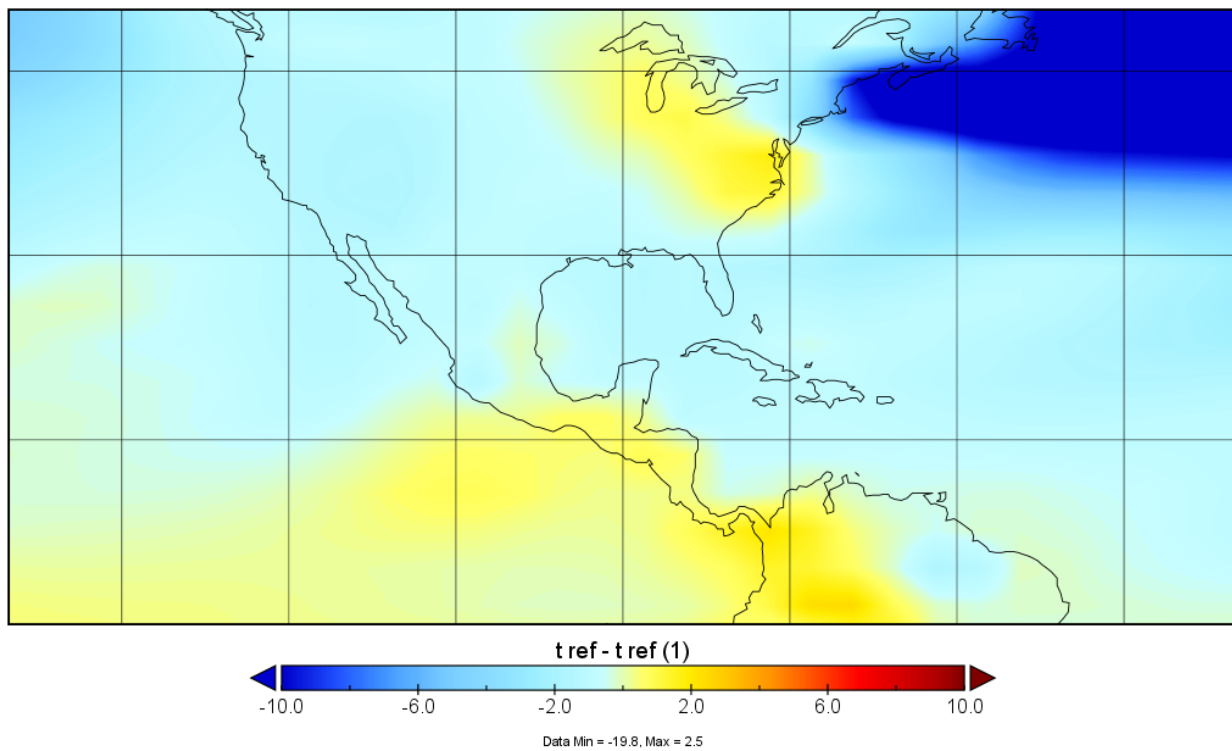
Hosed-unhosed in DJF, high orbital configuration, temperature anomaly



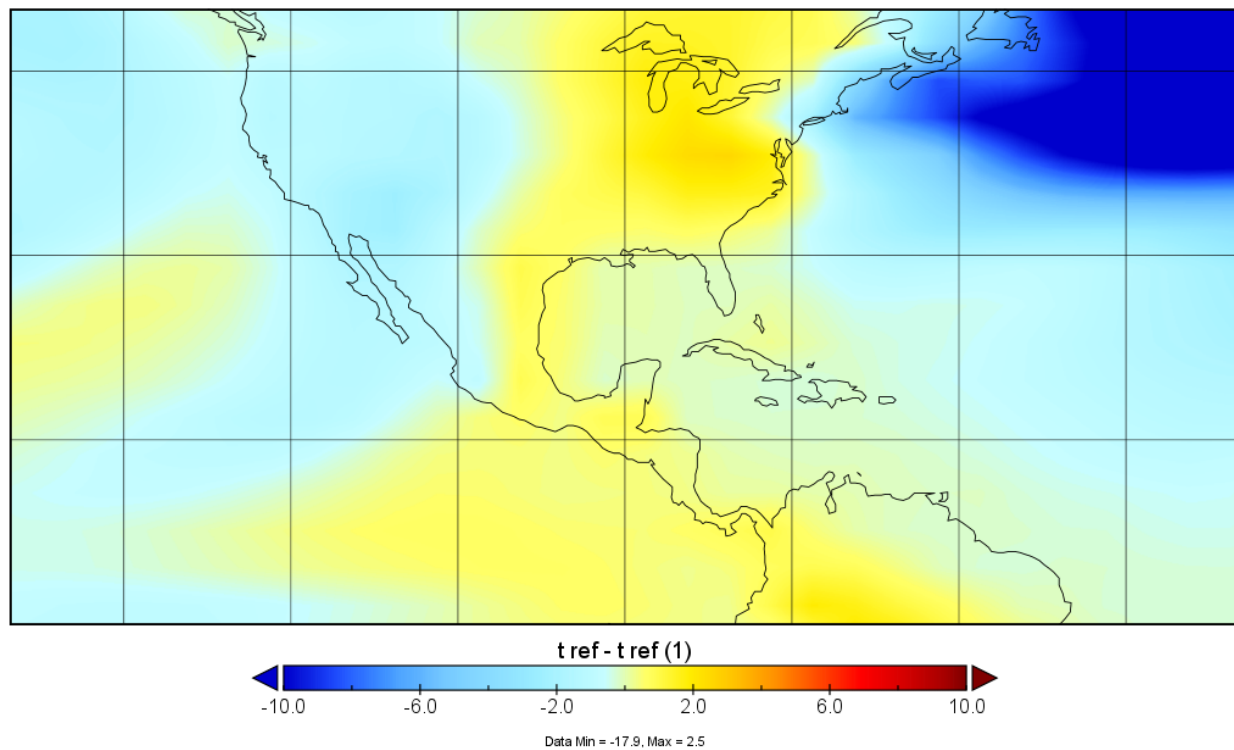
Hosed-unhosed in DJF, medium orbital configuration, temperature anomaly



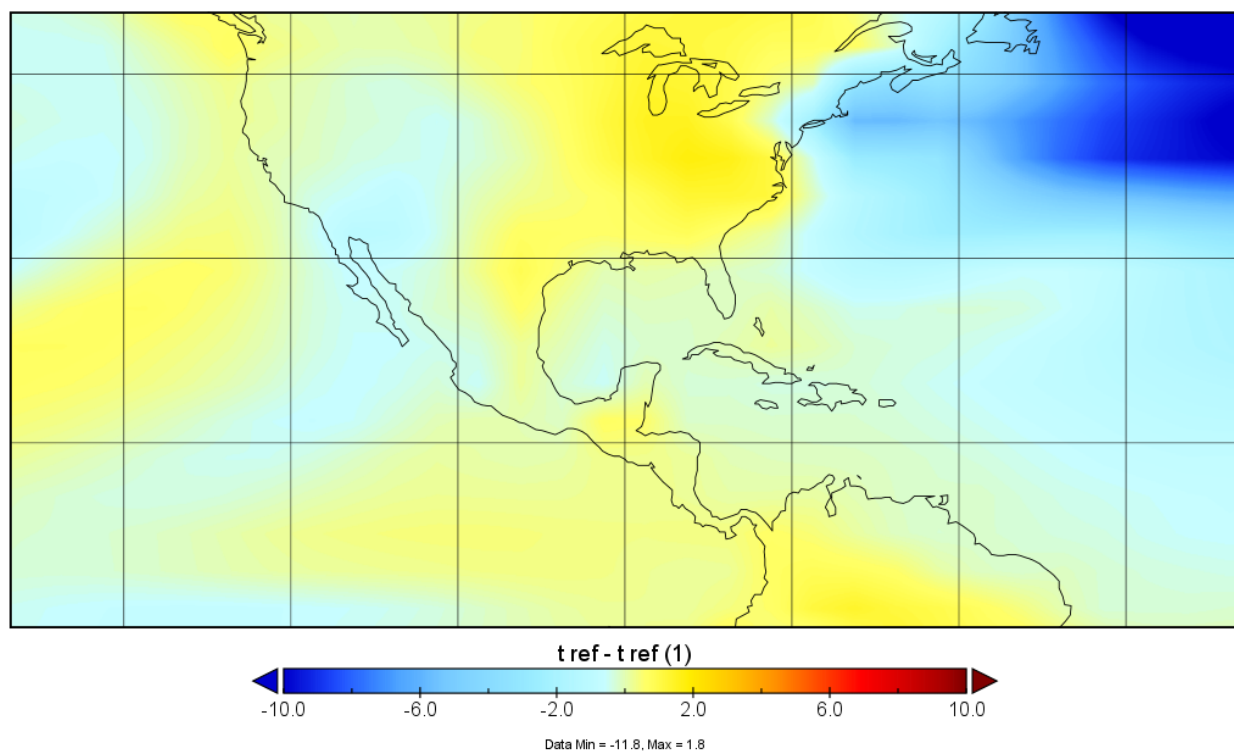
Hosed-unhosed in DJF, low orbital configuration, temperature anomaly



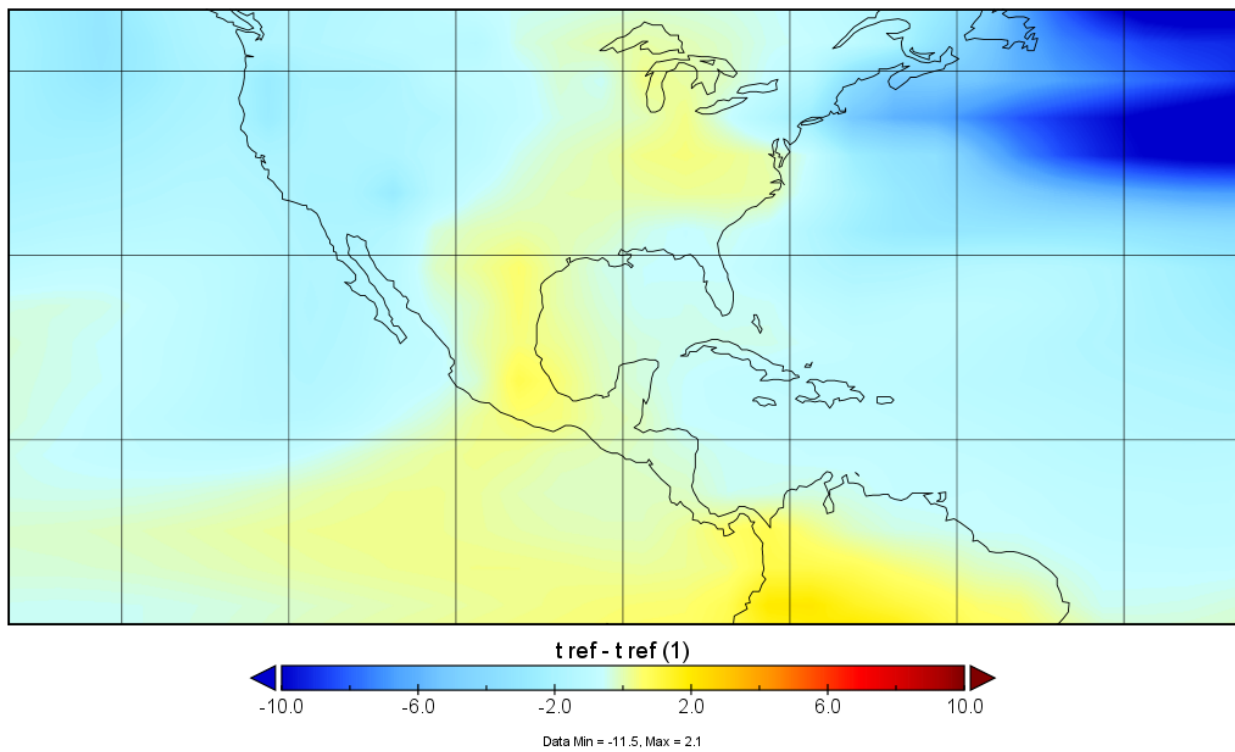
Hosed-unhosed in MAM, high orbital configuration, temperature anomaly



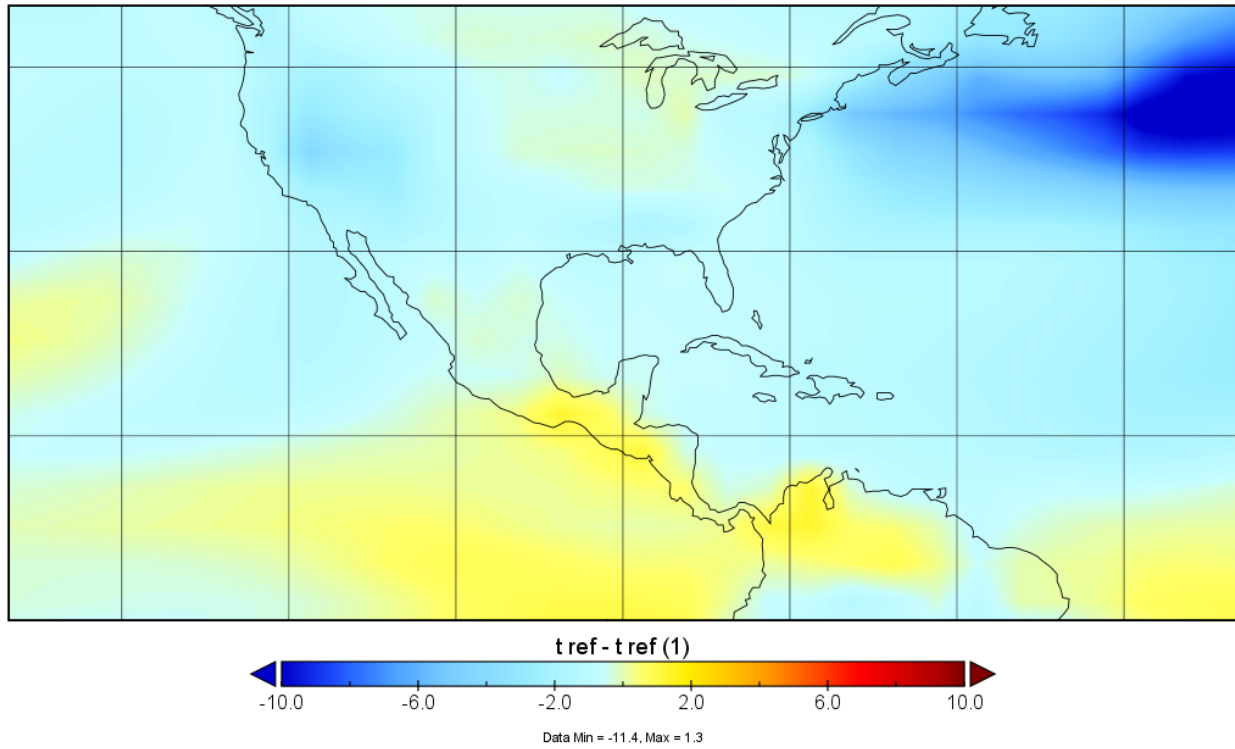
Hosed-unhosed in MAM, medium orbital configuration, temperature anomaly



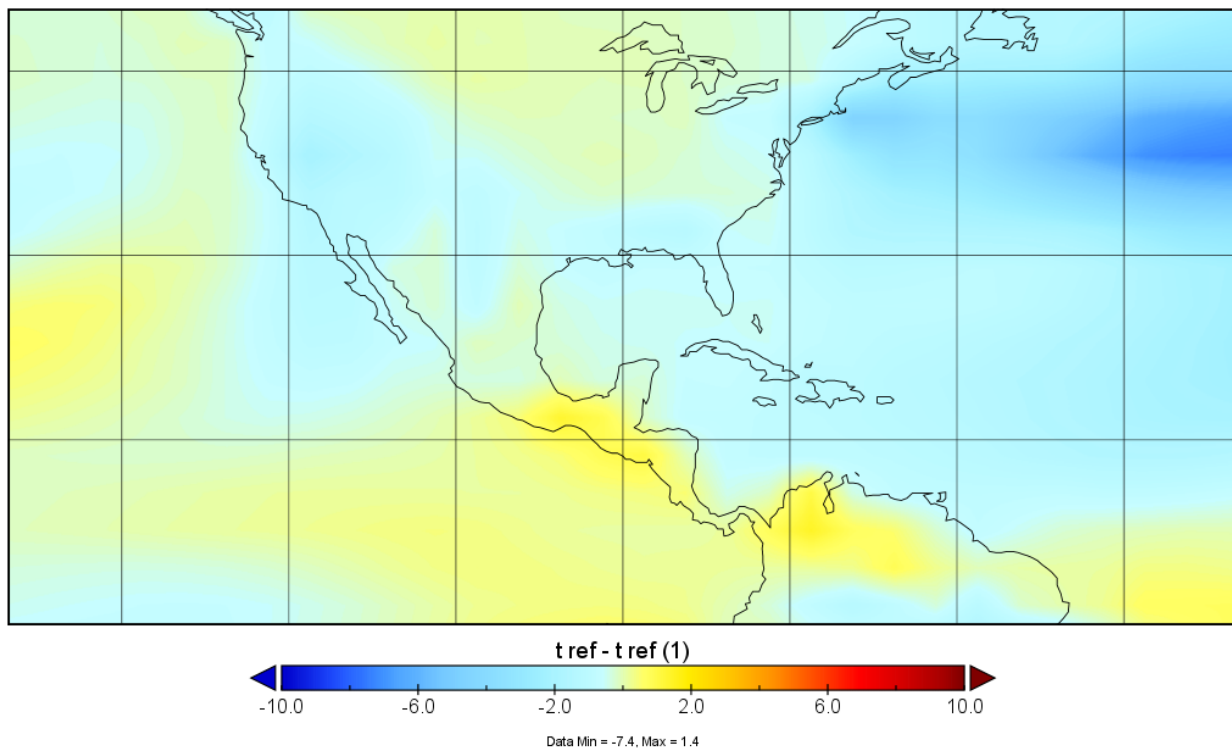
Hosed-unhosed in MAM, low orbital configuration, temperature anomaly



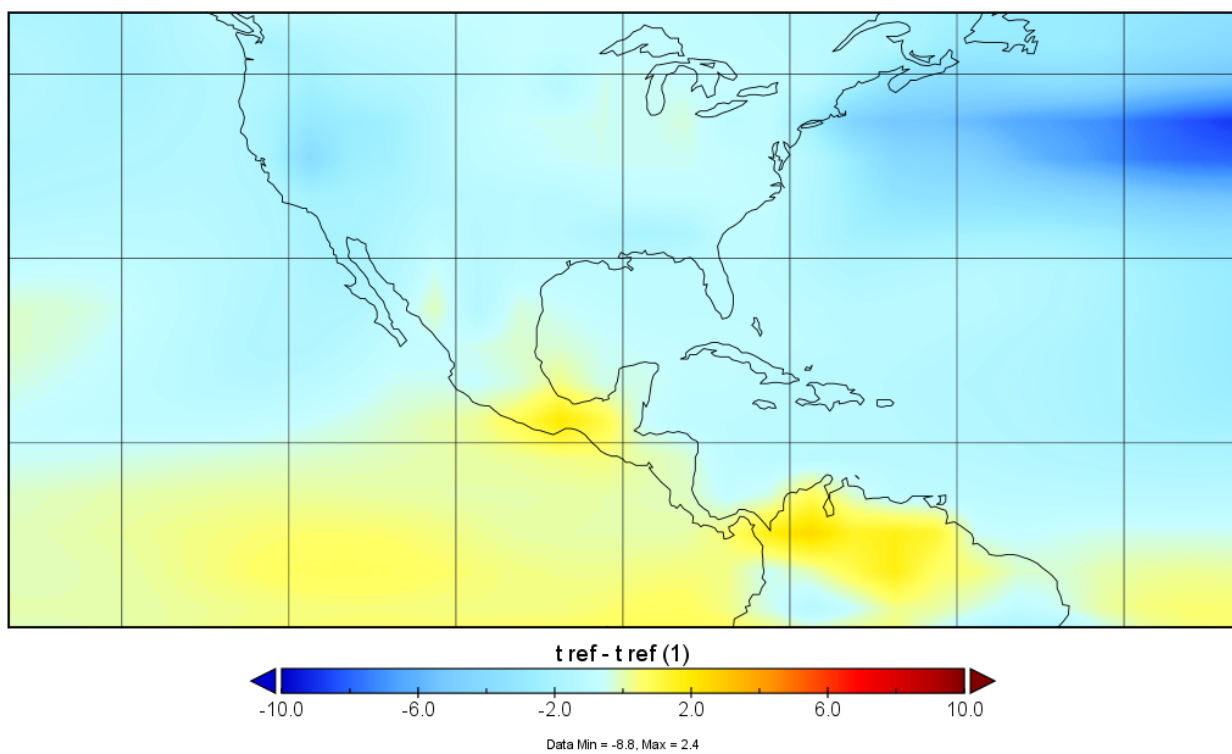
Hosed-unhosed in JJA, high orbital configuration, temperature anomaly



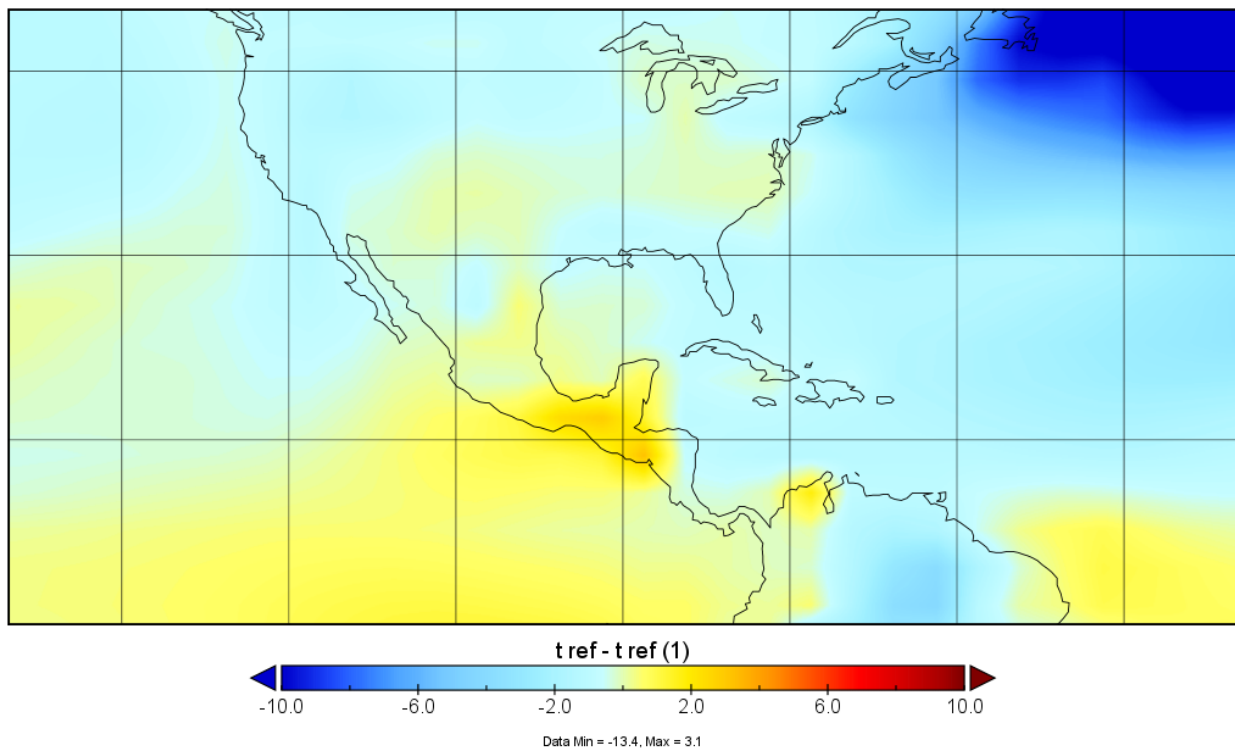
Hosed-unhosed in JJA, medium orbital configuration, temperature anomaly



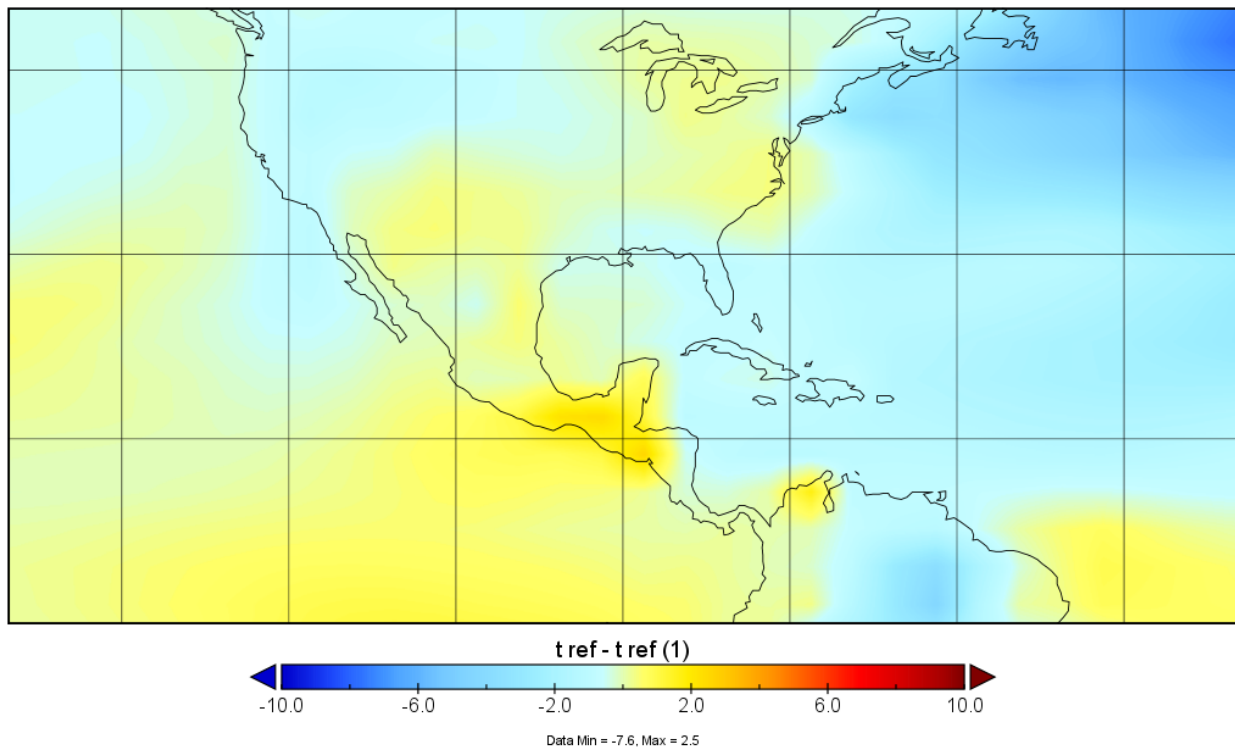
Hosed-unhosed in JJA, low orbital configuration, temperature anomaly



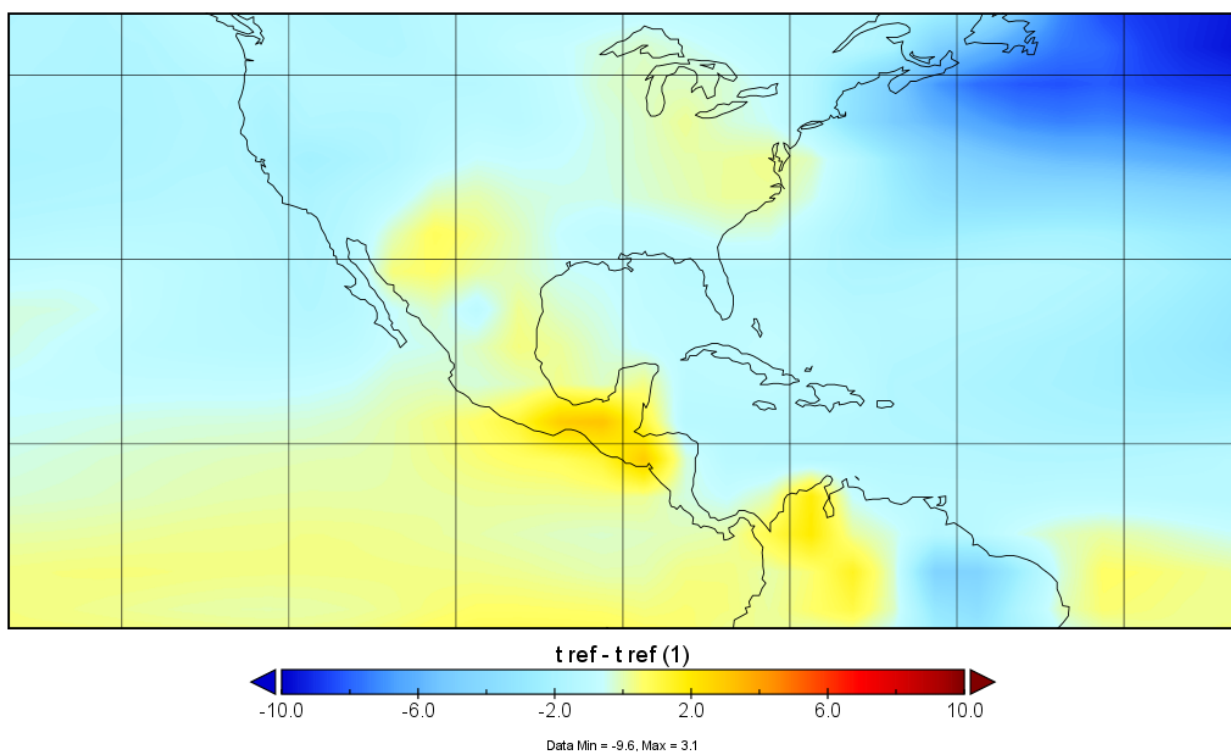
Hosed-unhosed in SON, high orbital configuration, temperature anomaly



Hosed-unhosed in SON, medium orbital configuration, temperature anomaly

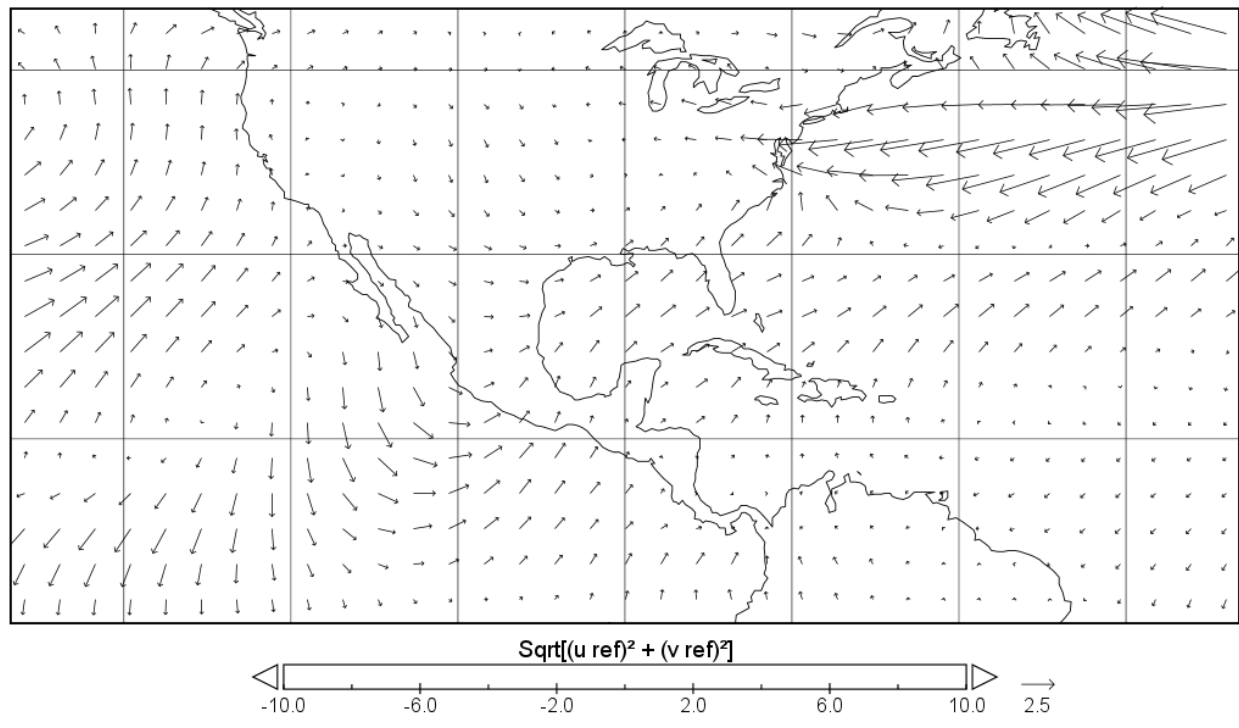


Hosed-unhosed in SON, low orbital configuration, temperature anomaly

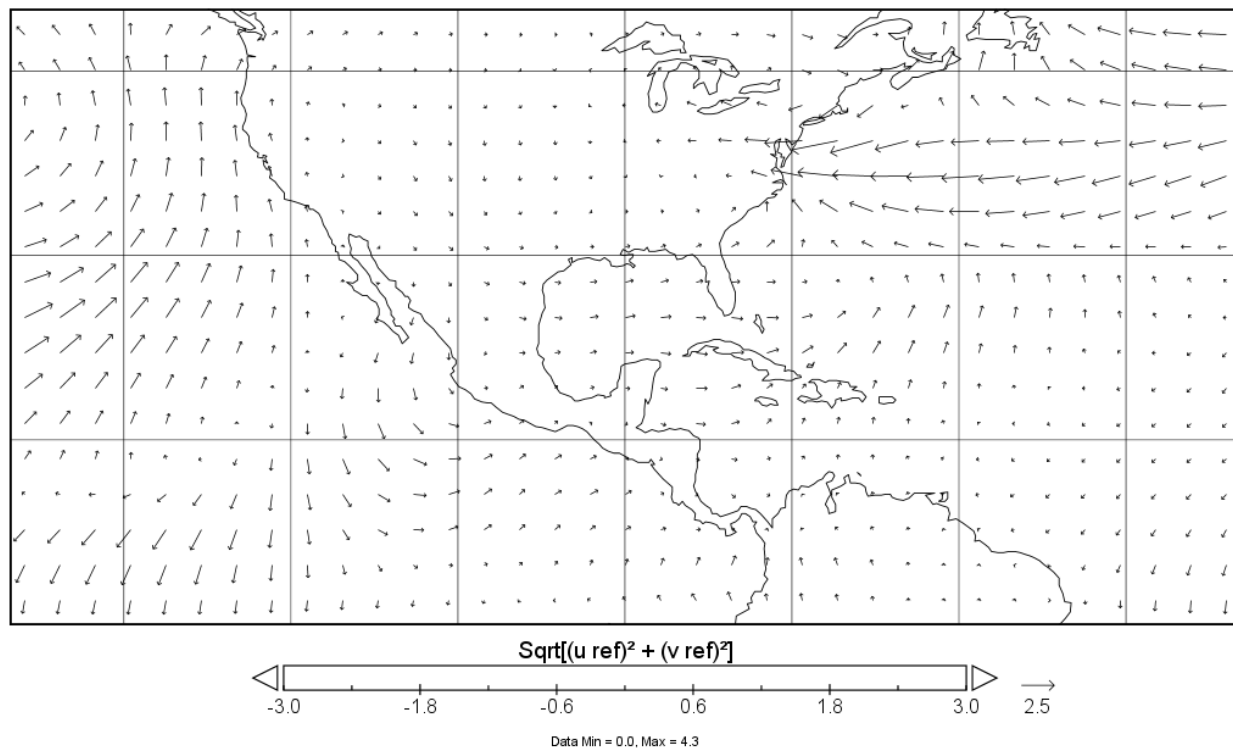


Wind

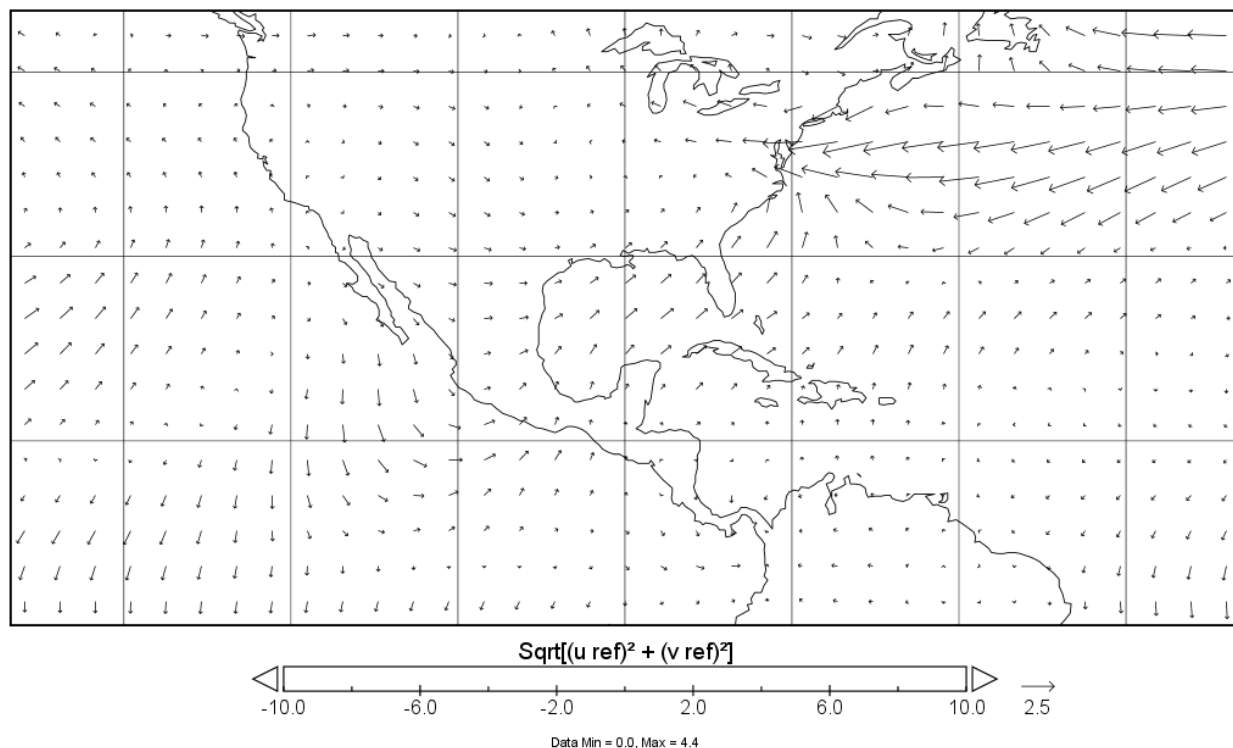
Hosed-unhosed in DJF, high orbital configuration, wind anomaly



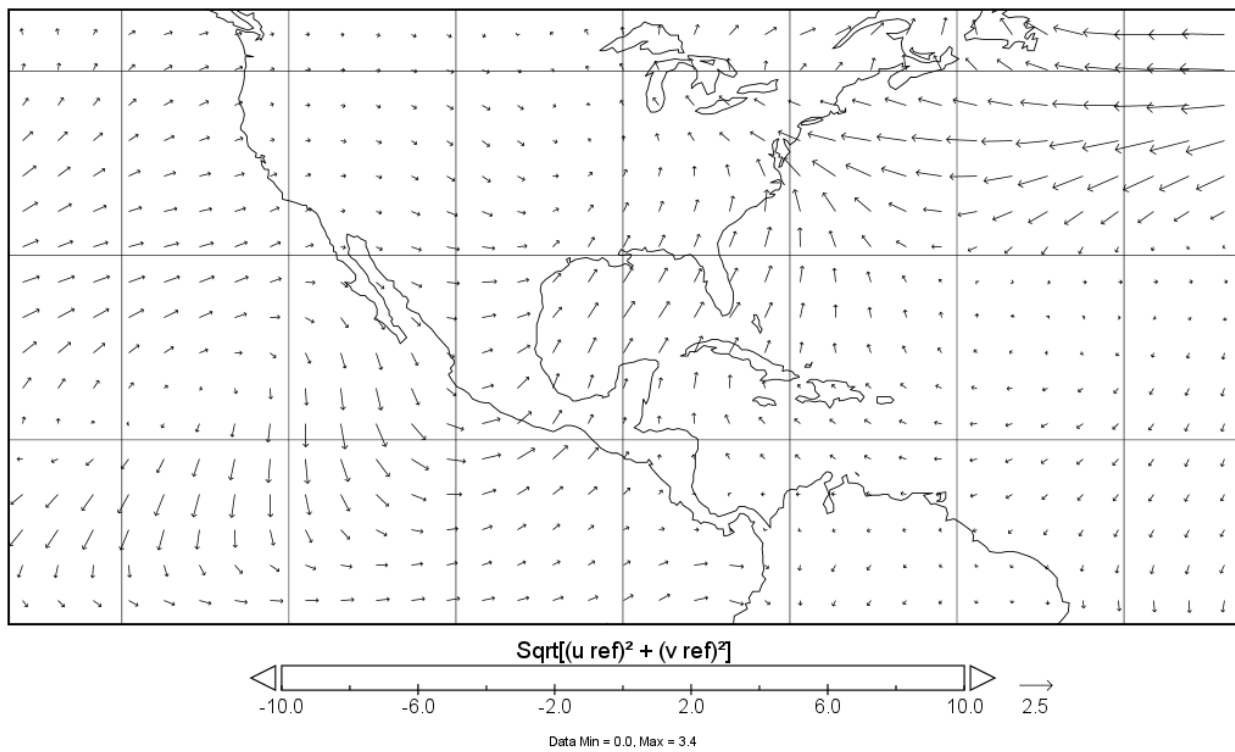
Hosed-unhosed in DJF, medium orbital configuration, wind anomaly



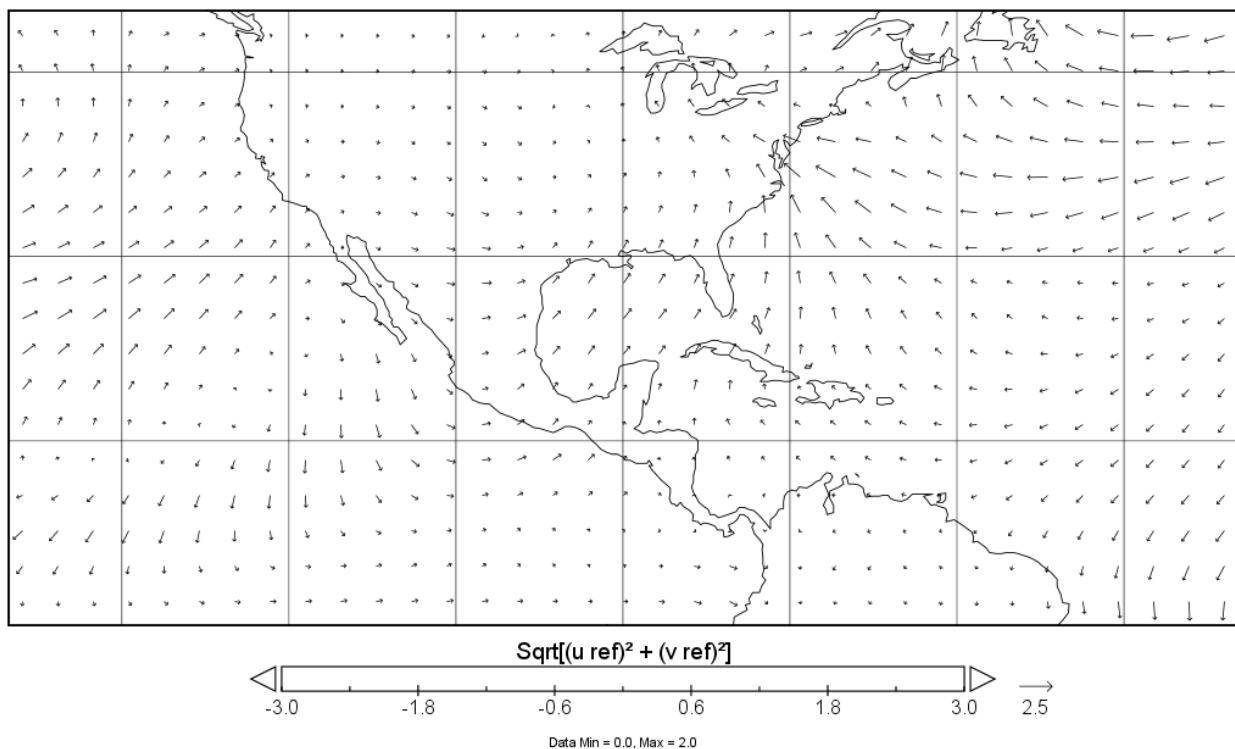
Hosed-unhosed in DJF, low orbital configuration, wind anomaly



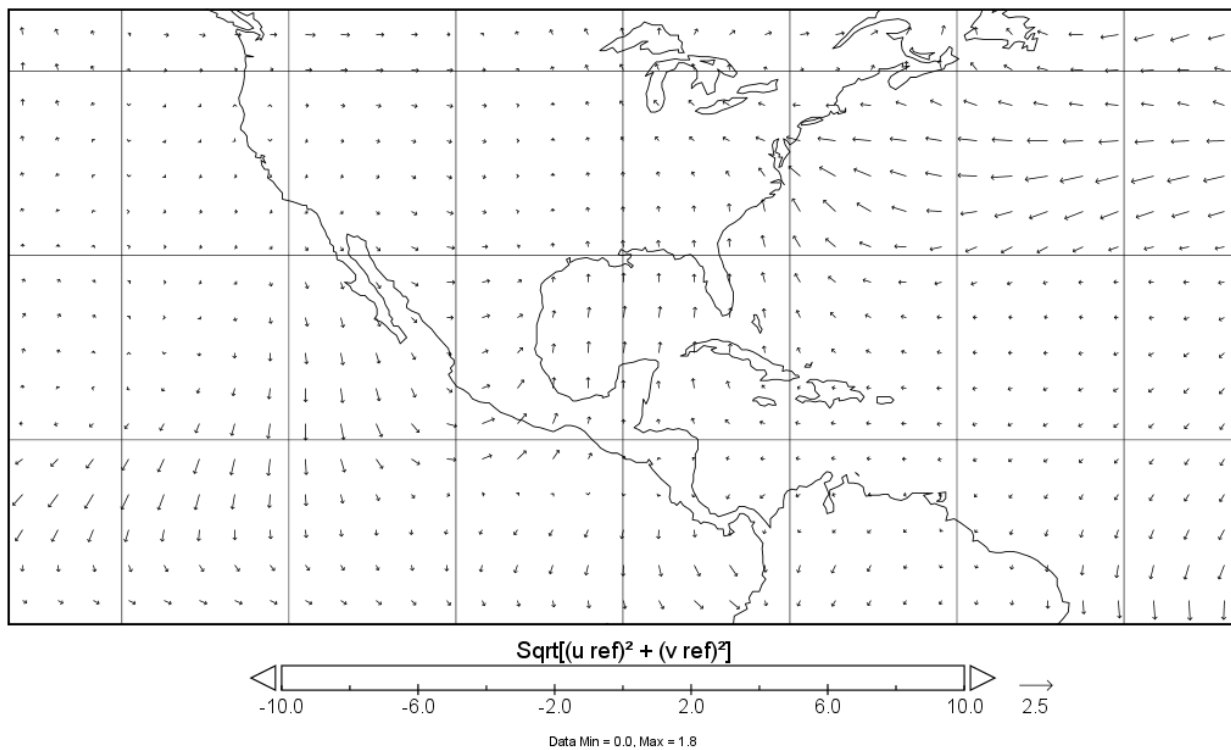
Hosed-unhosed in MAM, high orbital configuration, wind anomaly



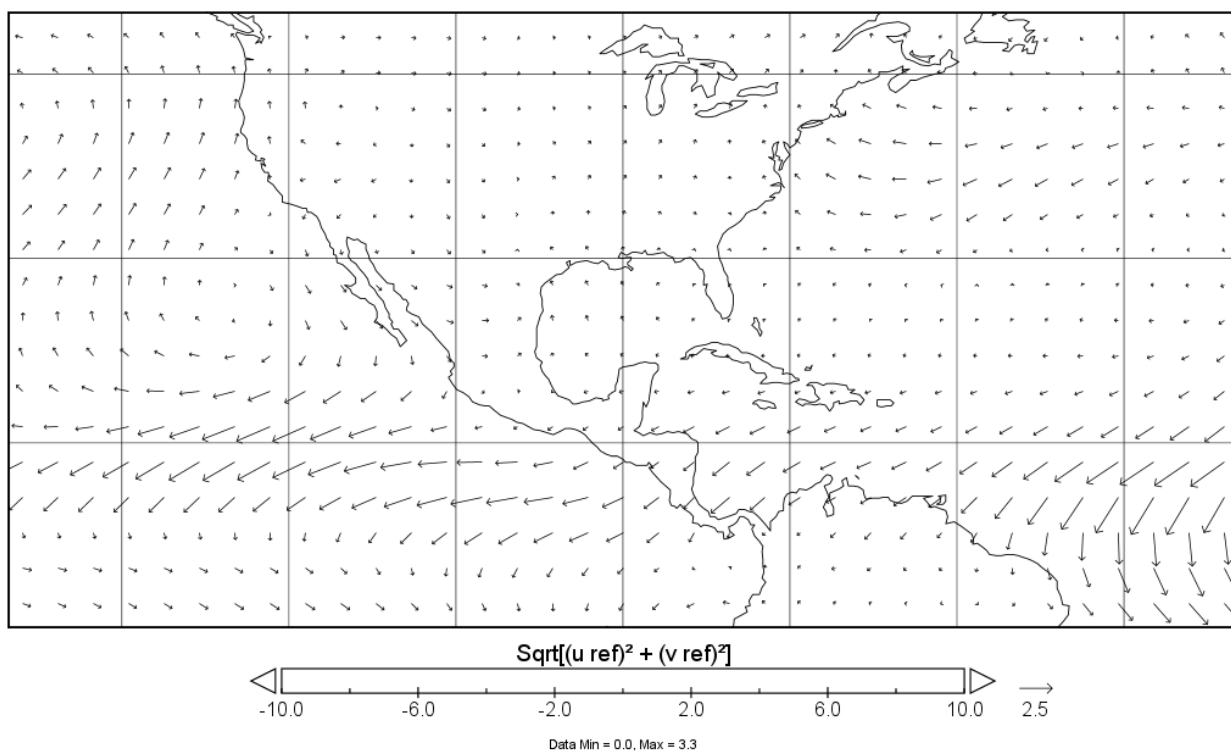
Hosed-unhosed in MAM, medium orbital configuration, wind anomaly



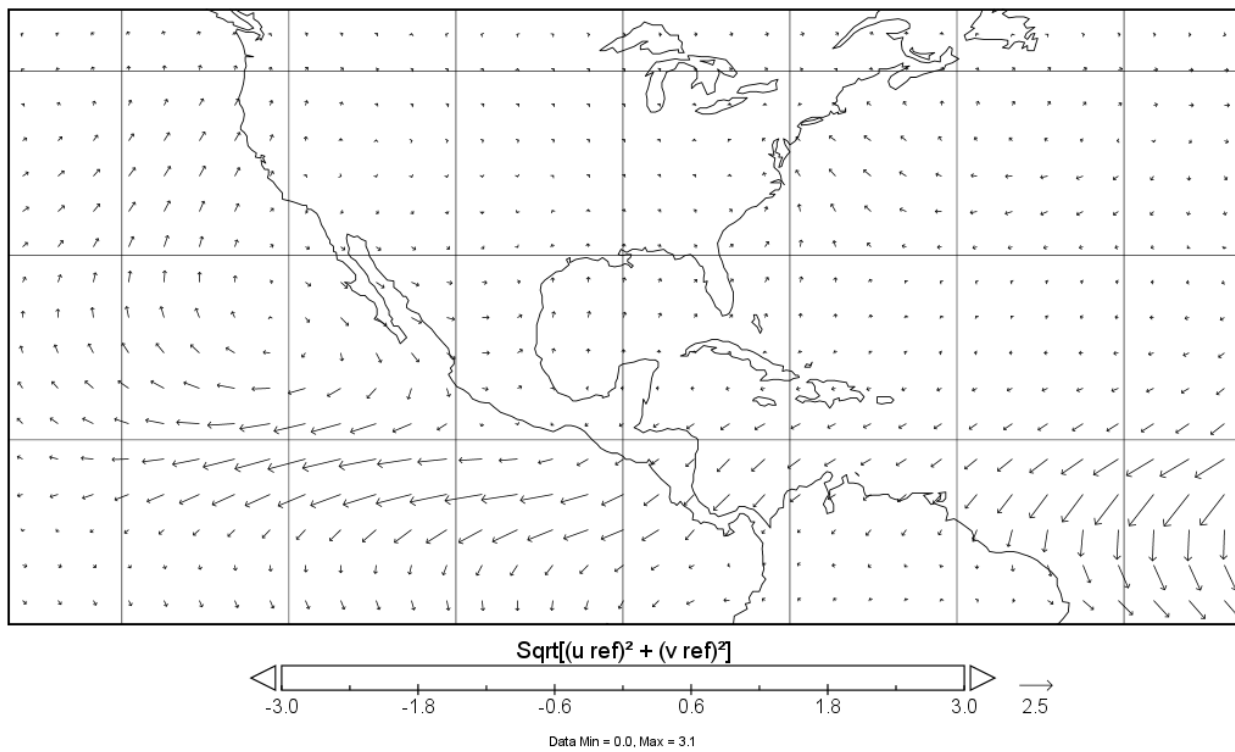
Hosed-unhosed in MAM, low orbital configuration, wind anomaly



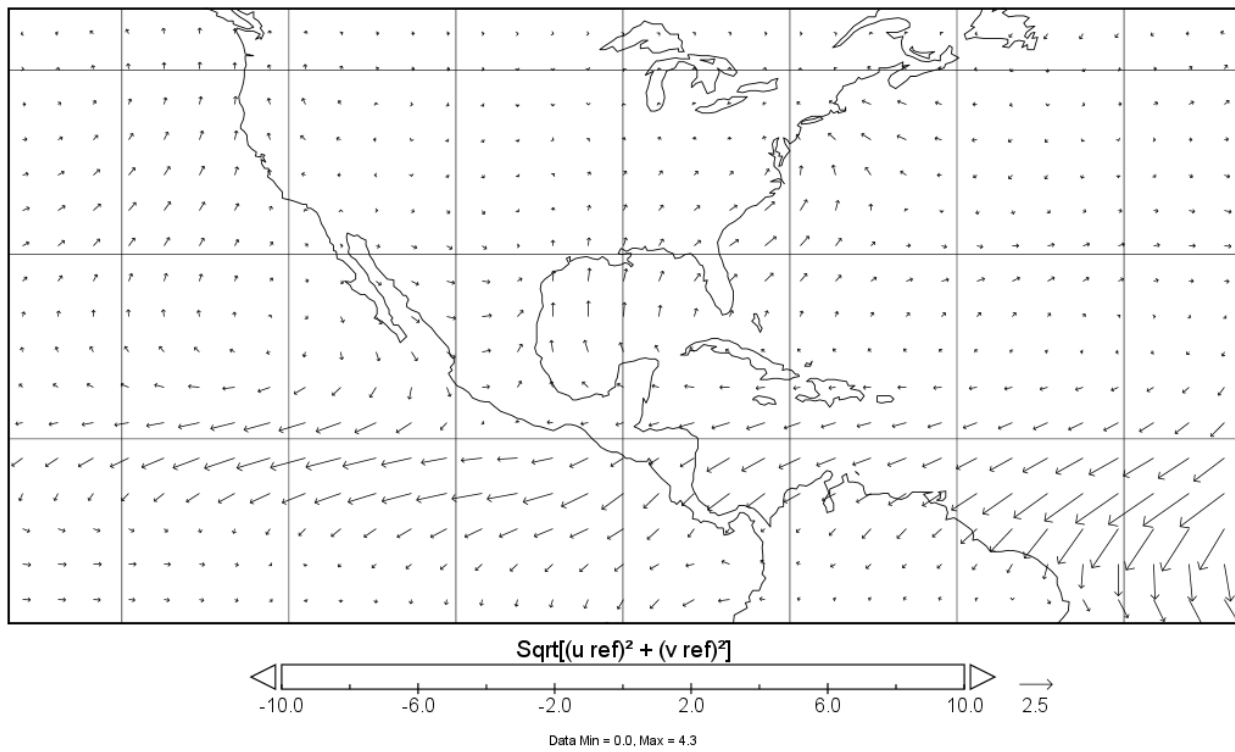
Hosed-unhosed in JJA, high orbital configuration, wind anomaly



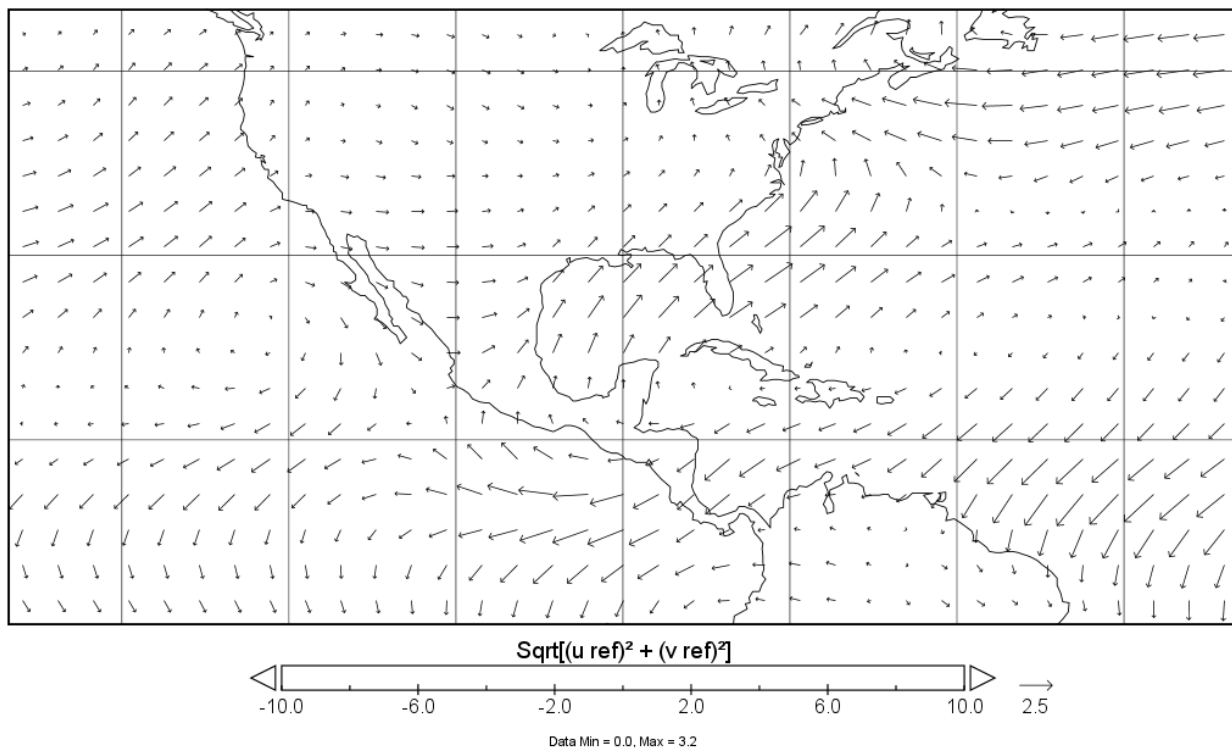
Hosed-unhosed in JJA, medium orbital configuration, wind anomaly



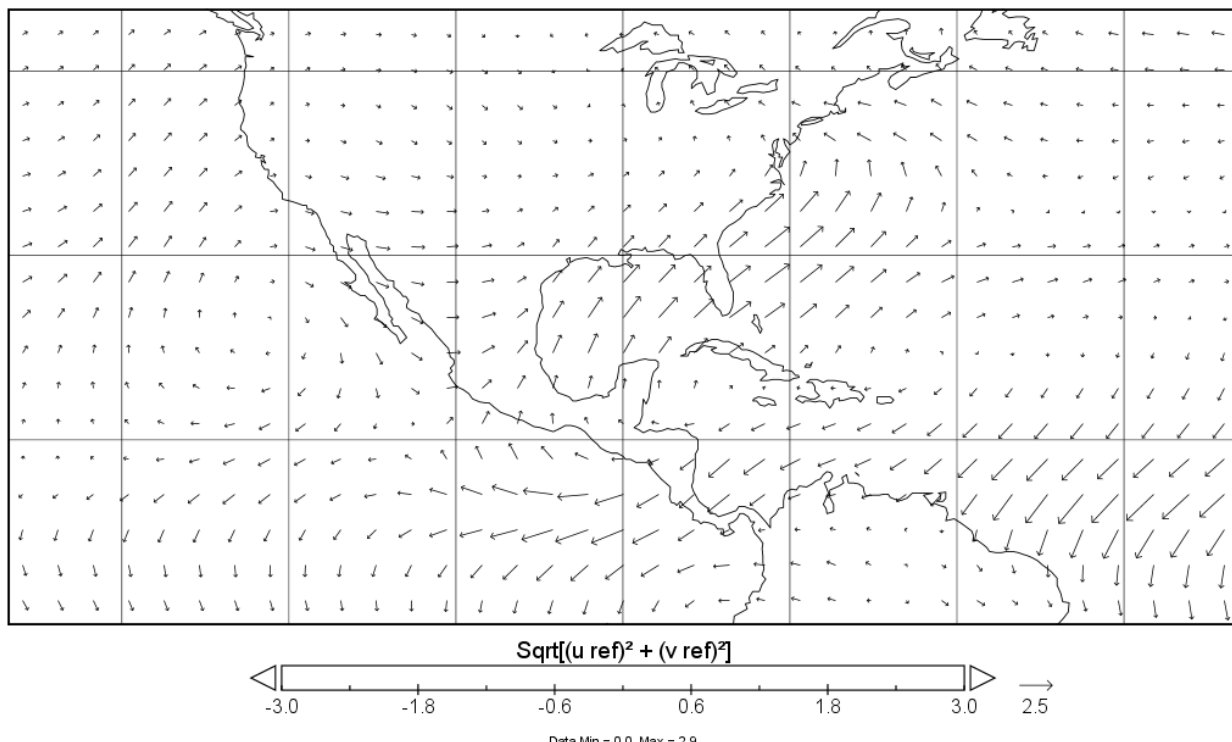
Hosed-unhosed in JJA, low orbital configuration, wind anomaly



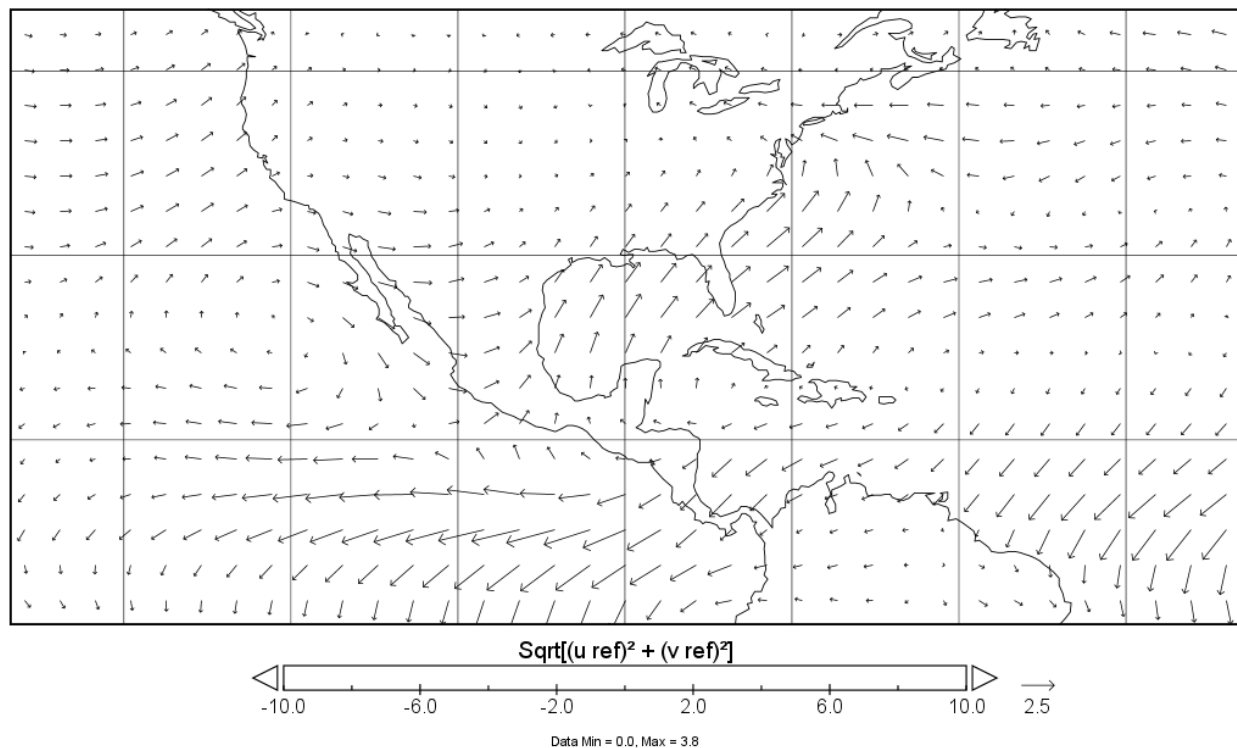
Hosed-unhosed in SON, high orbital configuration, wind anomaly



Hosed-unhosed in SON, medium orbital configuration, wind anomaly

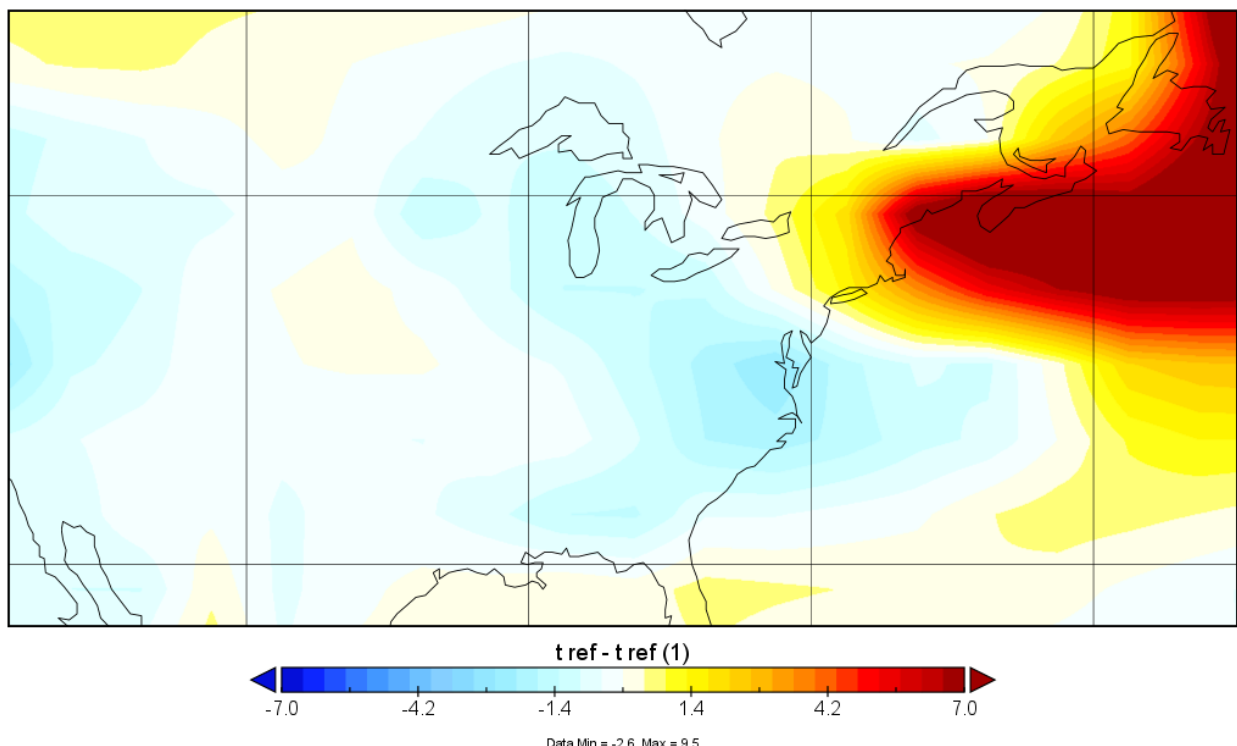


Hosed-unhosed in SON, low orbital configuration, wind anomaly

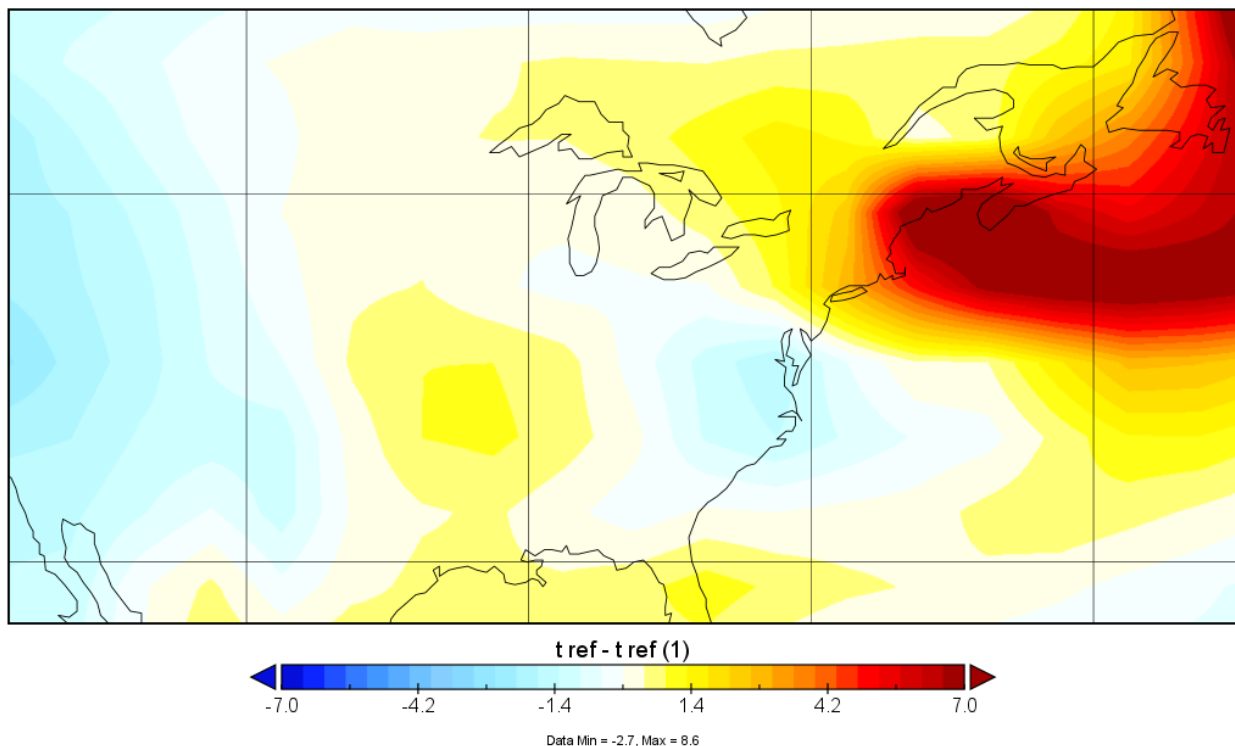


Difference between summer and winter temperature hosed-unhosed anomalies.

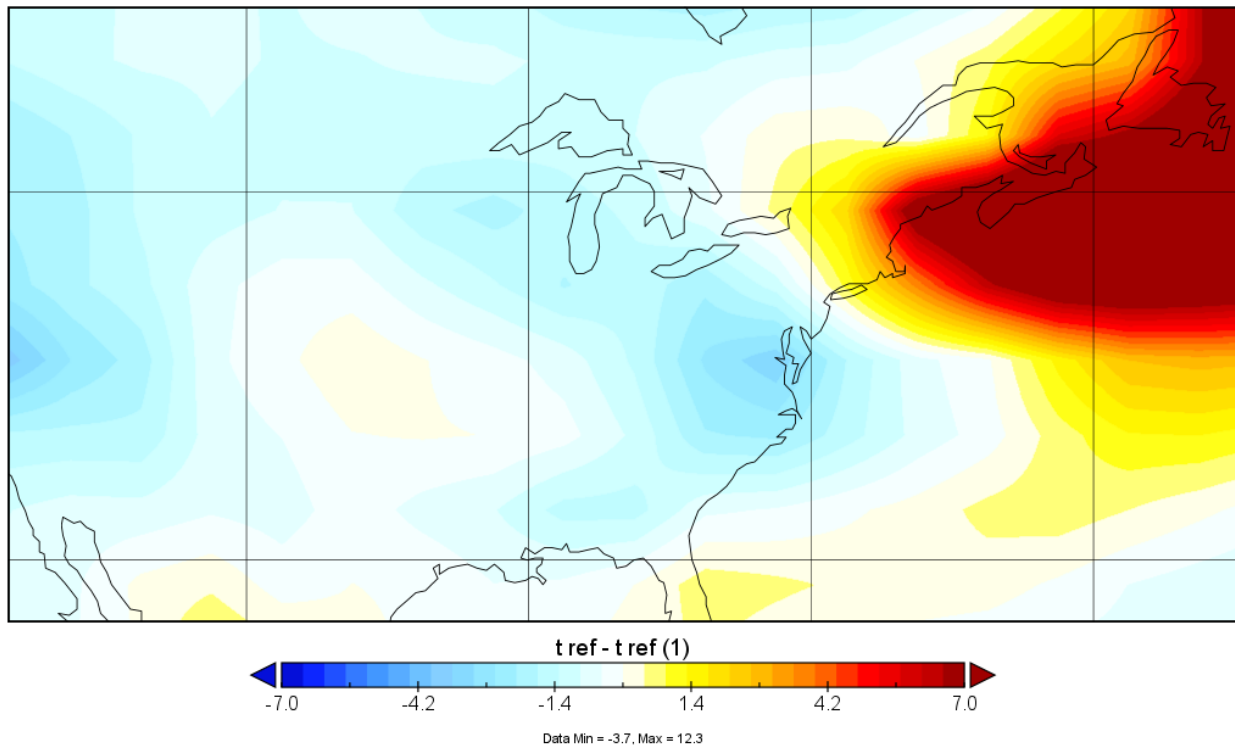
Temperature, Low Orbital Configuration



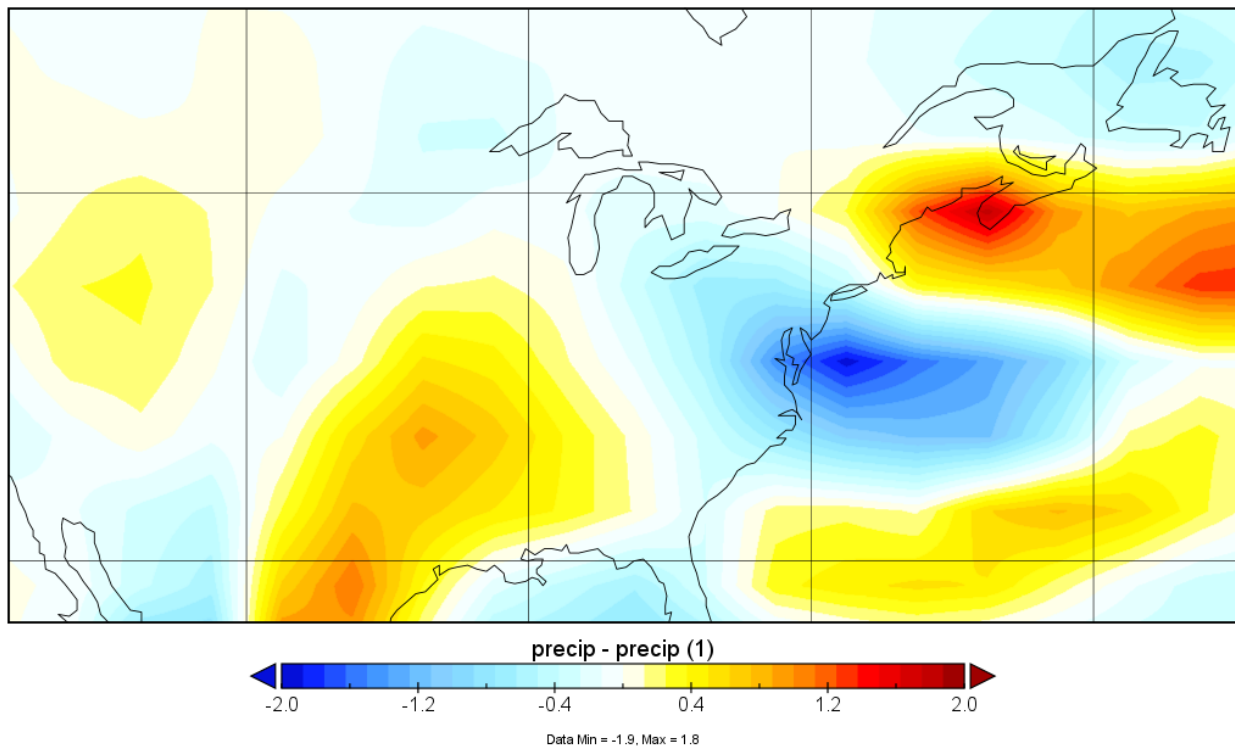
Temperature, Medium Orbital Configuration



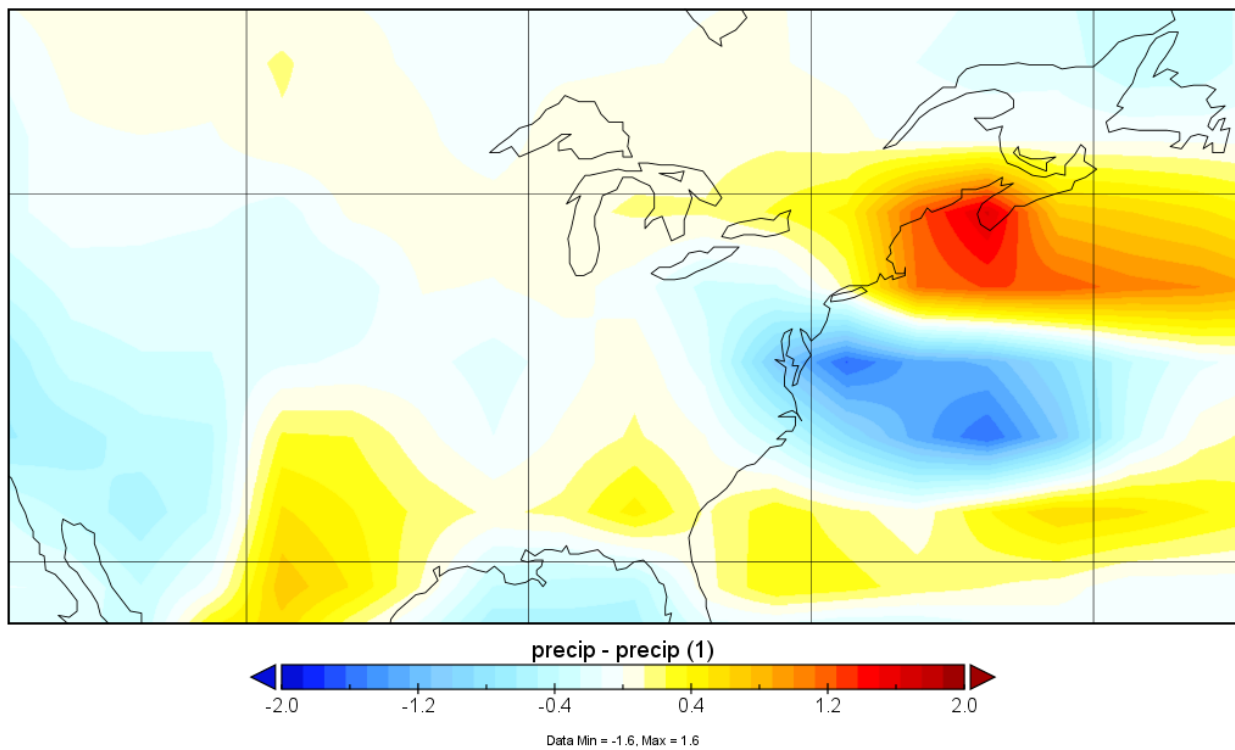
Temperature, High Orbital Configuration



Precipitation, Low Orbital Configuration



Precipitation, Medium Orbital Configuration



Precipitation, High Orbital Configuration

